# Experimental Study of Mechanical and Durability Properties in Hybrid Binary and Ternary Fiber-Reinforced ECC

Mahdi KouhiAzar Tulun<sup>1</sup>, Jafar Sobhani<sup>2\*</sup>, Seyyed Mohammad Mirhosseini<sup>3</sup>, Ehsanollah Zeighami<sup>4</sup> and Mohammad Reza Basiri<sup>5</sup>

1PhD student, Department of Civil Engineering, Arak Branch, Islamic Azad University, Arak, Iran Email: mahdi.kouhiazartulun@iau.ac.ir

2Associated Professor, Department of Concrete Technology, Road, Housing & Urban Development Research Center (BHRC), Tehran, Iran.

Corresponding author: Jafar Sobhani; Email: <a href="mailto:sobhani@bhrc.ac.ir">sobhani@bhrc.ac.ir</a>
3Associated Professor, Ph.D., Department of Civil Engineering, Arak Branch, Islamic Azad University, Arak, Iran.

Email: m-mirhoseini@iau-arak.ac.ir

4Assistant Professor, Ph.D., Department of Civil Engineering, Arak Branch, Islamic Azad University, Arak,

Email: e-zeighami@iau-arak.ac.ir

5Assistant Professor, Ph.D., Department of Textile Engineering, Arak Branch, Islamic Azad University, Arak, Iran

Email: m-basiri@iau-arak.ac.ir

#### Abstract

This research introduces an innovative approach to producing high-performance engineered cementitious composites (ECC) using hybrid fibers. By integrating steel, synthetic, and PVA fibers, the composites achieved a 40% increase in compressive strength, reaching 94.8 MPa at 28 days, alongside a 9.5% improvement in flexural strength, with the ternary mixture S20F10P2 showing the best performance. They also experienced a 31% increase in tensile strength, measuring 8.99 MPa for S10F20P2. The hybrid fibers further enhanced energy absorption, boosting flexural toughness by 20% (120 N.mm for S20F10P2) and promoting multiple microcracking behaviors, effectively limiting crack widths to around 60 micrometers. In durability tests, the ECC demonstrated excellent resistance to water penetration, with a depth of 3.5 mm for S10F0P2, mass loss of 4.4 gr/m² during freeze-thaw cycles for S0F0P0, and chloride ion ingress of 87 coulombs for the fiberless mixture. Additionally, incorporating ground granulated blast furnace slag (GGBFS) and silica fume as cement replacements improved mechanical performance and reduced CO<sub>2</sub> emissions by 338.2 kg/m³, highlighting the environmental benefits of these materials. The results demonstrated that incorporating hybrid binary and ternary fiber systems significantly enhanced ECC's compressive, tensile, and flexural performance and toughness while maintaining favorable durability characteristics. These findings indicate strong potential for utilizing the developed composite mixtures in industrial and public concrete overlay applications. The findings pave the way for eco-friendly construction practices and advancements in sustainable concrete technology.

**Keywords-** Engineered Cementitious Composites (ECC), Mechanical Response, Energy Absorption, Pavement Overlay, Hybrid steel-synthetic-PVA fibers, Supplementary Cementitious Material (SCM).

#### 1. Introduction

Concrete is globally recognized as one of the most essential building materials and is widely used in constructing various structures and road infrastructures. However, unreinforced concrete has limitations, including low flexural and tensile strength, limited toughness, large crack widths, and brittle behavior under tensile and flexural loading. The increasing demand for advanced civil infrastructure has led to a significant rise in concrete and cement consumption, resulting in the depletion of natural resources and substantial carbon dioxide emissions. Research

International Journal of Multiphysics Volume 18, No. 4, 2024

ISSN: 1750-9548

indicates that cement production accounts for approximately 5 to 7% of global greenhouse gas emissions [1-4]. While fiber-reinforced concretes (FRCs) partially address these issues, they still exhibit softening tensile behavior and limited ductility [5].

Strain-hardening cementitious composites (SHCCs), also known as engineered cementitious composites (ECC), have been developed to overcome these challenges. ECCs employ a unique failure management strategy that ensures efficient fiber distribution, enhancing crack resistance and superior toughness [6]. Introduced in the 1990s by Lee and his colleagues, ECCs are a specialized category of ultra-high-performance fiber-reinforced concrete (UHPFRC) based on micromechanical theory [7-10]. Unlike conventional concrete, ECC exhibits strain-hardening behavior after initial cracking, similar to ductile metals, with a strain capacity 300 to 500 times greater than regular concrete. Additionally, ECC demonstrates superior crack width control under loading, with microcracks propagating uniformly and stabilizing at approximately 60 micrometers due to its micromechanical design [11]. The exclusive use of fine sand in ECC formulations further enhances strain capacity and promotes multiple cracking [12-14]. However, the absence of coarse aggregates in ECC results in higher cement consumption, often exceeding 1000 kg/m³ in standard formulations [15]. Although ECC shows promise for structural applications, its relatively lower compressive strength than other concrete materials remains a limitation [16,17]. Enhancing compressive strength and modulus of elasticity while maintaining adequate plasticity could significantly improve its effectiveness, as these properties are critical for structural design [18].

Concrete overlays are vital in improving pavement structural performance by addressing fatigue and durability issues caused by prolonged service life. The mechanical properties of these overlays directly influence the performance of restored pavements. Engineered cementitious overlays, characterized by high strength and flexibility, offer superior performance. Investigating the properties of composite overlays with various fiber types is essential for optimizing their application in pavement repair [4,19-22].

The hybridization of different fiber types has been shown to enhance tensile strength and toughness in concrete [4,21-23]. Macro-synthetic fibers, for instance, improve the mechanical properties of concrete [4], while combining polyethylene and steel fibers enhances ECC's flexural, compressive, and tensile strength [24]. Including varying-sized fibers effectively controls crack propagation and distribution in concrete [25-27]. Increasing the steel fiber content in concrete boosts compressive strength and tensile modulus [28]. Similarly, the combination of polyethylene (PE) and steel fibers positively impacts the tensile strength of high-performance concrete [26]. However, incorporating steel fibers alongside PVA fibers reduces the tensile strain capacity of ECC.

In contrast, the combination of PVA and basalt fibers enhances it due to the strong bonding properties of basalt fibers [30]. The hybrid use of steel and polyethylene fibers in ECC improves performance under repeated loading and effectively controls crack width during flexural loading [31]. Combining steel and polyethylene fibers enhances ECC's tensile strain capacity and resistance [31]. Studies have also demonstrated that the hybrid use of PE and PVA fibers significantly improves the mechanical properties of ECC [33]. Combining steel and PVA fibers has enhanced cracking resistance and flexural performance [6].

Fibers are categorized into two categories based on size: microfibers and macrofibers. Microfibers, typically 6 to 20 mm in length and tens of microns in diameter, have limited impact on structural performance under large deformations. In contrast, macrofibers, ranging from 30 to 60 mm long and over 0.3 mm in diameter, provide load-bearing capacity and control visible cracks, similar to reinforcing bars, after matrix failure [34].

The global concrete production exceeds 10 billion tons annually, with each ton of Portland cement production releasing approximately one ton of carbon dioxide into the atmosphere [35,38]. The extensive use of riverbed sand as fine aggregate in concrete has led to environmental degradation, including riverbed erosion and increased vulnerability to floods and storms [34]. ECC, which eliminates the need for coarse aggregates, offers a sustainable alternative. However, its higher cement content than conventional concrete increases costs and carbon emissions [3]. To reduce this issue., supplementary cementitious materials (SCMs) such as granulated blast furnace slag (GGBFS) [39-41] and silica fume [41-44] can be used as partial replacements for cement. Research has shown that incorporating GGBFS and silica fume enhances the compressive strength of ECC [44].

A key innovation of this research is the incorporation of GGBFS and silica fume to reduce cement consumption, thereby addressing environmental concerns associated with carbon dioxide emissions. This research aims to evaluate hybrid fiber's simultaneous effects on the fresh, hardened, and durability properties of ECC containing these fibers in binary and ternary combinations by experimental tests demonstrated in Fig. 1.

ISSN: 1750-9548

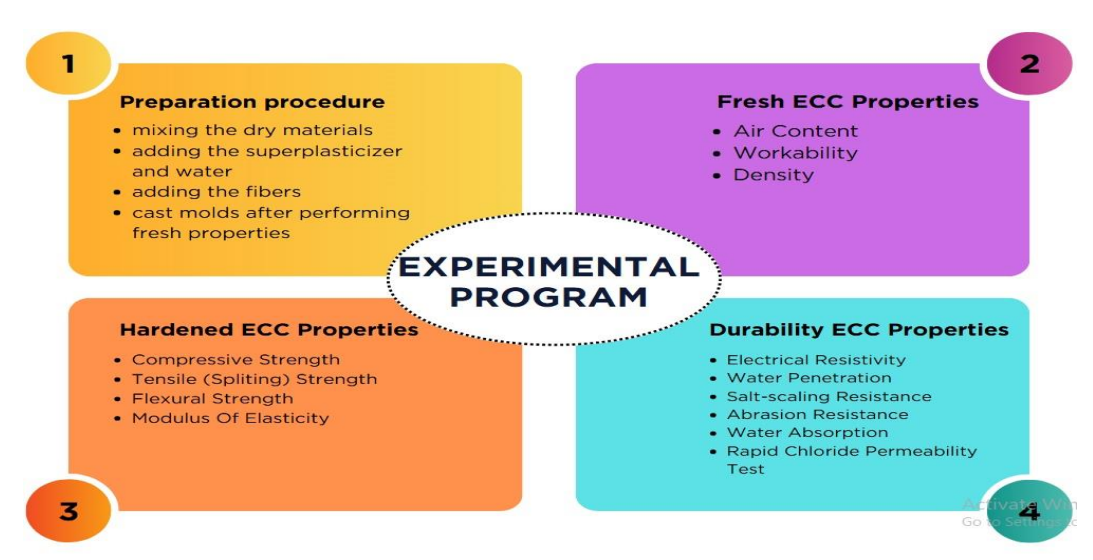


Fig. 1. Experimental program detail.

#### 2. Materials

In this experimental study, industrial by-products, including silica fume (SF) and ground granulated blast furnace slag (GGBFS), were used in conjunction with ordinary Portland cement (OPC), silica sand, and micro silica to create engineered cementitious composites (ECC). Images of the raw materials are presented in Fig. 2. The mechanical properties of the cement are summarized in Table 1, and the chemical compositions of the ordinary Portland cement, micro silica, silica fume, and ground granulated blast furnace slag are detailed in Table 2. A polycarboxylate-based superplasticizer was included to ensure the mixture's workability, with its specifications outlined in Table 3. The polycarboxylate superplasticizer was specifically selected for this study due to its superior performance characteristics in fiber-reinforced ECC. Its steric hindrance mechanism provides excellent water reduction while maintaining prolonged workability, which is critical for ensuring proper fiber distribution without segregation. The anionic carboxylate groups create strong electrostatic repulsion between cement particles, significantly improving the dispersion of hybrid fibers and preventing fiber balling that a common issue in high fiber content mixes. Furthermore, three types of fibers — steel, synthetic, and polyvinyl alcohol (PVA) — were utilized in this study. Additionally, Fig. 3 displays the results of the grain size analysis for the ordinary Portland cement (OPC), silica sand, micro silica, silica fume (SF), and ground granulated blast furnace slag (GGBFS), along with their corresponding curves. The microsilica byproduct (2-30 µm) from silica sand crushing effectively fills voids between cement and sand particles, reducing porosity and creating a denser ECC matrix. Images of the fibers are presented in Fig. 4, and their properties are listed in Table 4. Table 5 illustrates the ECC mixtures formulated for the experimental procedures.



Fig. 2. Used material: (a) silica fume, (b) GGBFS, (c) cement, (d) micro silica, (e) silica sand.

Table 1. Mechanical properties of cement.

Tuote 1. Medianical properties of centeria	
Properties	Value
Fineness	300
Initial setting time (min)	40
Final setting time (h)	7
3 Days age compressive strength (MPa)	10
7 Days age compressive strength (MPa)	16
28 Days age compressive strength (MPa)	32

Table 2. Chemical properties of SF, GGBFS, cement, and micro silica.

Chemical	SF (%)	GGBFS (%)	Cement (%)	Micro silica
$SiO_2$	90.36	37.82	22.33	98
CaO	0.83	37.8	61.45	0.3
$Al_2O_3$	0.43	12.58	4.8	1.05
$Fe_2O_3$	0.58	1.35	3.5	0.4
MgO	0.89	4.89	2.7	0.18
K2O	1.46	0.41	0.62	0.9
Na2O	0.66	0.33	0.37	0.5
So3	-	0.62	2.4	0.02

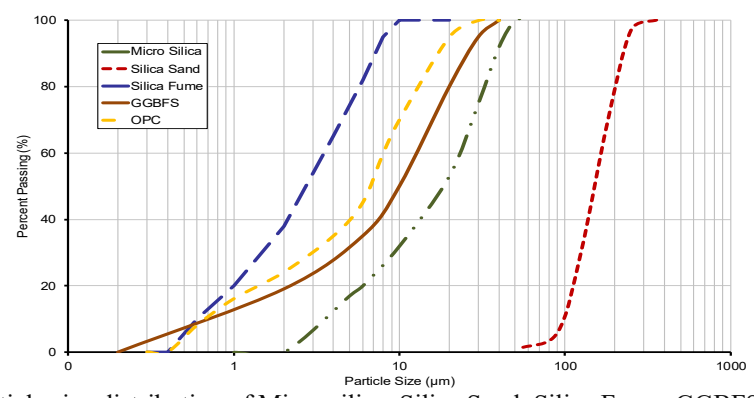


Fig. 3. Particle size distribution of Micro silica, Silica Sand, Silica Fume, GGBFS, and OPC.

Table 3. Chemical properties of superplasticizer.

Table 3. Chemical properti	es of superplasticizer.
Properties	Value
Appearance	Liquid- white
Chloride ion	Less than 0.1%
pH	6.5–7.5
Freezing point	2 °C



Fig. 4. The shape of fibers. (a) PVA Fiber; (b) Synthetic fiber; (c) Hooked steel Fiber.

Table 4. Specifications of the utilized fibers.

Properties	PVA fiber	Synthetic fiber	Steel fiber
Length (mm)	12	60	60
Diameter (mm)	0.04	0.4-0.5	0.9
Tensile strength (MPa)	1400	660-570	1600
Modulus of elasticity (GPa)	32	6	200
Density(gr/cm <sup>3</sup> )	1.3	0.9	7.85

Table 5. Mixtures proportions of ECC \* (Unit: kg/m3).

ID	Mixture	PVA fiber (%)	Synthetic fiber (%)	Steel fiber (%)
R	S0F0P0	0	0	0
B1	S10F0P1	1 (0.05)	0	10 (0.5)
B2	S10F0P2	2 (0.1)	0	10 (0.5)
В3	S20F0P1	1 (0.05)	0	20 (1)
B4	S20F0P2	2 (0.1)	0	20 (1)
B5	S0F10P1	1 (0.05)	10 (0.5)	0
В6	S0F10P2	2 (0.1)	10 (0.5)	0
В7	S0F20P1	1 (0.05)	20 (1)	0
В8	S0F20P2	2 (0.1)	20 (1)	0
T1	S10F10P1	1 (0.05)	10 (0.5)	10 (0.5)
T2	S20F10P1	1 (0.05)	10 (0.5)	20 (1)
Т3	S10F20P1	1 (0.05)	20 (1)	10 (0.5)
T4	S10F10P2	2 (0.1)	10 (0.5)	10 (0.5)
T5	S20F10P2	2 (0.1)	10 (0.5)	20 (1)
Т6	S10F20P2	2 (0.1)	20 (1)	10 (0.5)

\*W/C (OPC+GGBFS+SF) = 0.2; Cement: 700; Silica fume: 50; GGBFS: 350; Silica sand: 500; Micro Silica: 200; Water: 220.

# 3. Experimental program

# 3.1. Mixing Process

The mixing procedure was carefully designed to ensure homogeneous fiber distribution and optimal workability. A planetary mixer with a capacity of 50 liters was utilized at a constant speed of 120 rpm. The dry components, including Type II Portland cement and silica sand, blended for 3 minutes. Approximately 80% of the mixing water

ISSN: 1750-9548

containing a polycarboxylate-ether-based superplasticizer was gradually added over 2 minutes. The pre-mixed fibers were slowly introduced in 30-second intervals while the speed of the mixer was decreased. to 60 rpm to prevent balling. The mixture underwent final wet mixing for 3 minutes at 150 rpm, with periodic visual inspections confirming uniform fiber dispersion without clumping.

## 3.2. Casting and Curing

The samples were prepared according to ASTM C31 [45] and cured following ASTM C511 [46] standards. Cubic and cylindrical specimens were cast in steel molds in three equal layers, with each layer receiving 25 strokes of rod compaction. Immediately after casting, all specimens were covered with damp burlap and polyethylene sheets and stored in a temperature-controlled room (25±2°C) for 24 hours as specified in ASTM C31 [46]. Following demolding, the specimens were transferred to a lime-saturated water curing tank maintained at conditions prescribed by ASTM C511 [46] (23±2°C) until testing ages 7, 28, and 90 days.

## 3.3. Evaluating the homogeneity of mixtures

Fig. 5(a) shows the fresh mixed ECC, and Fig. 5(b) demonstrates the surface visual inspections, emphasizing the homogeneity of the produced ECC samples.

Moreover, Fig. 6 (a-e) depicts SEM photomicrographs of ECC, emphasizing the well-distribution of natural and cement matrix in the ECC mixture.

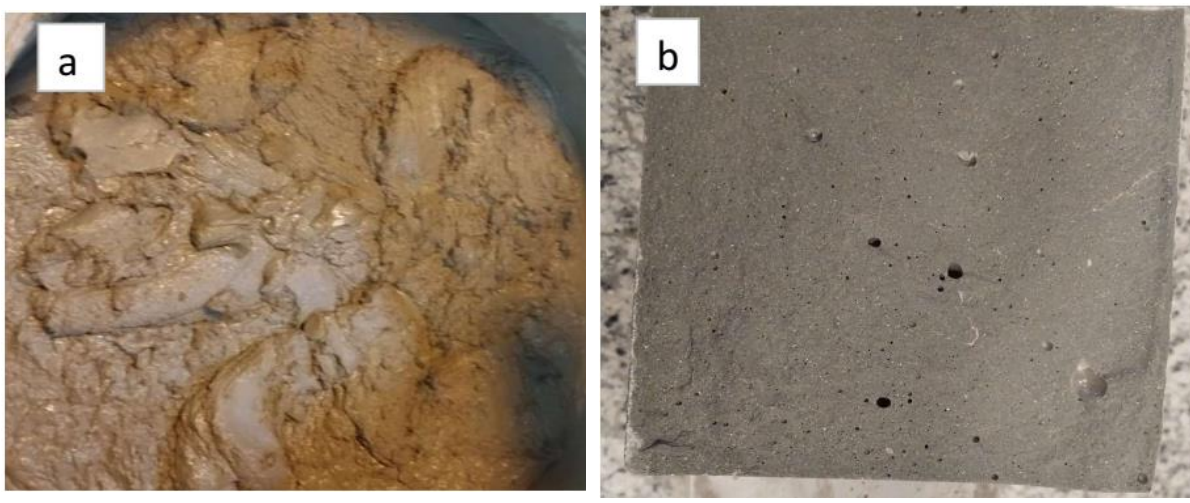
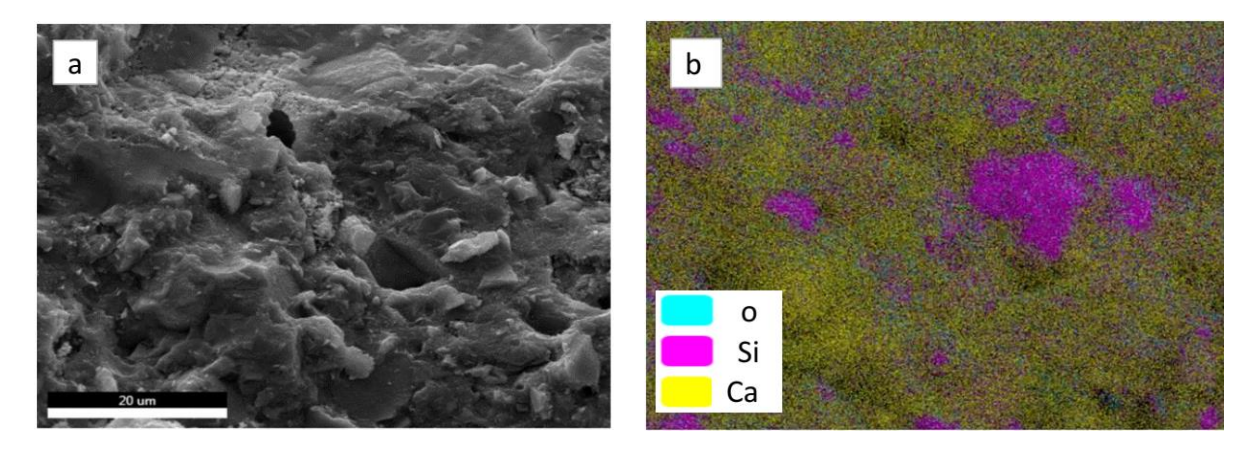


Fig. 5. (a) Fresh mixed ECC; (b) Surface visual inspection for mixture homogeneity.



ISSN: 1750-9548

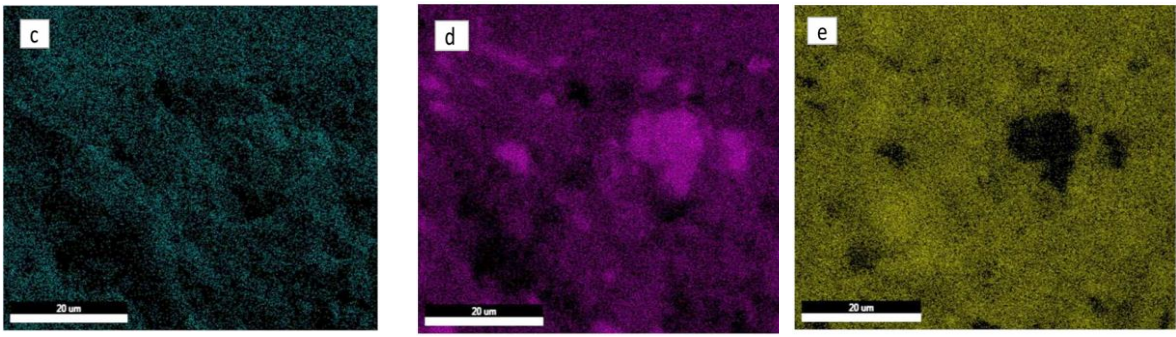


Fig. 6. SEM photomicrographs of (a): Mixture, (b): Distribution of oxygen(o), Silica(Si), and Calcium(Ca) (c): Oxygen (O), (d): Silica (Si), (e): Calcium (Ca).

# 3.4. Test procedure

#### 3.4.1. Properties of fresh ECC

The properties of the fresh ECC, such as specific weight, unintended air entrainment percentage, and mini-slump flow, were investigated. The research studies carried out these tests to evaluate the workability and density characteristics of the fresh ECC, which are critical for its application in construction projects. The Significance of Mini-Slump Tests in ECC Mixture: The average of two perpendicular diameters has been reported as the minislump value of each mix (Fig. 7(a)). The test to determine the air content percentage of the engineered cementitious composite will conducted by ASTM C231 [47] (Fig. 7(b)). Additionally, the specific weight measurement of the engineered cementitious composite will performed following ASTM C138 [48] (Fig. 7(c)).

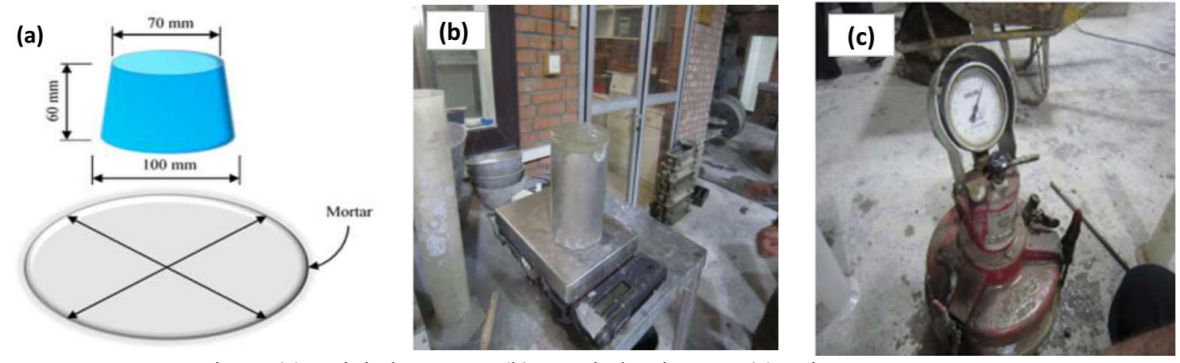


Fig. 7. (a): Mini-slump test, (b): Fresh density test, (c): Air content percentage test.

# 3.4.2. Compressive strength test

Prepared Cubic specimens with  $100 \times 100 \times 100$  mm dimensions were for compressive strength testing. For each mixture, three samples were cast and tested at curing ages of 7, 28, and 90 days in compliance with the BS EN 12390-3 standard [49]. Determined the compressive strength by applying a constant loading rate of  $0.6 \pm 0.2$  N/mm²/s. An initial preload (approximately 30% of the anticipated failure load) is used to seat the specimen to ensure accurate measurements. Following this, the load was increased continuously and smoothly at the specified rate ( $\pm 10\%$  tolerance) to prevent any shock or sudden impact until the specimen reached its maximum load-bearing capacity. This method ensured precise and reliable evaluation of the compressive strength of the engineered cementitious composites (ECC).

# 3.4.3. Flexural performance test

The flexural strength of the engineered cementitious composites (ECC) was evaluated using prismatic beam specimens with dimensions of  $150 \times 150 \times 550$  mm by the ASTM C1609M-19a standard [50] (Fig. 8). The tests were conducted at the age of 28 days under third-point loading conditions to simulate realistic stress distribution. A controlled loading rate of 0.1 mm/min was applied to ensure a gradual and consistent increase in load, minimizing any potential impact or shock. The specimens were continuously loaded until failure, and the maximum applied load was recorded in kilonewtons (kN). Three replicate samples were tested for each mixture, and the average flexural strength was calculated and reported as the representative value.

ISSN: 1750-9548

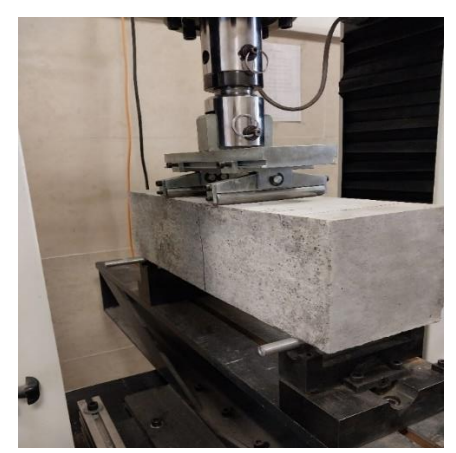


Fig. 8. Flexural beam specimens testing.

# 3.4.4. Tensile (splitting) strength test

The engineered cementitious composites (ECC) tensile splitting strength was evaluated using cylindrical specimens with a diameter of 150 mm and a height of 300 mm by the ASTM C496 standard [51]. The tests were conducted at the age of 28 days to assess the tensile behavior of the material. Three replicate samples were tested for each mixture, and the average tensile splitting strength was calculated and reported as the representative value. This testing protocol ensured accurate and reliable measurement of the tensile properties of the ECC.

## 3.4.5. Modulus of elasticity

The mixtures' modulus of elasticity and cylindrical specimens with dimensions of  $150 \times 300$  mm were prepared and tested by ASTM C469 [52]. The specimens underwent axial loading, measuring stress and strain within the elastic range. The modulus of elasticity was calculated as the slope of the linear portion of the stress-strain curve. The tests were conducted under controlled temperature and constant relative humidity to ensure high accuracy and repeatability of the results.

# 3.4.6. Water Penetration Resistance

The water penetration resistance of ECC was evaluated following the EN 12390-8 standard [53] (Fig. 9(a)). Specimens were tested under water pressure to measure their resistance to water ingress. Lower penetration depths indicate enhanced durability, particularly in moisture-exposed environments.

## 3.4.7. Water Absorption

The water absorption of ECC was determined by DIN EN 1338 [54]. Specimens were dried, immersed in water, and weighed regularly to calculate the percentage of water absorption. Lower water absorption values indicate reduced porosity and enhanced durability, particularly in environments prone to moisture exposure.

# 3.4.8. Abrasion Resistance Test (Rotating-Cutter Method)

DIN EN 1338 [54] evaluated ECC's abrasion resistance using the rotating-cutter method (Fig. 9(b)). Samples were subjected to a rotating cutter under a specified load, and the wear length was measured after a set of 28 cycles. Lower mass loss values indicate superior abrasion resistance, highlighting the material's suitability for high-traffic surfaces and industrial applications.





Fig. 9. (a) Water Penetration, (b) Wide wheel abrasion test machine.

ISSN: 1750-9548

## 3.4.9. Freeze-Thaw Resistance with Deicing Salts

The salt scaling of the ECC mixtures was determined according to EN 1338 [54] with a 3% NaCI solution. At the end of freeze-thaw cycles, the mixtures were collected and weighed to determine their mass loss (ML) as a salt-scaling resistance measure (Fig. 10).



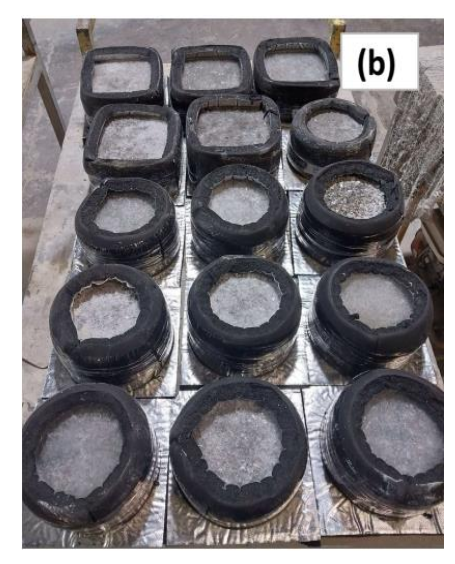


Fig. 10. (a) Salt-scaling test, (b) ECC mixture tested.

# 3.4.10. Chloride Ion Penetration Resistance

The chloride ion penetration resistance of ECC was evaluated by ASTM C1202 [55] (Fig. 11(a)). The specimens were exposed to an electrical potential, and the total charge that passed through them was measured. Lower charge values indicate reduced chloride ion permeability, highlighting the material's durability in marine environments or areas exposed to deicing salts.

# 3.4.11. Surface Resistivity Test (SR)

AASHTO T358 [56] measured the electrical resistivity of ECC using the four-point probe method (Fig. 11(b)). This test evaluates the material's ability to resist the passage of electrical current, directly related to its permeability and durability. Higher resistivity values indicate lower permeability and enhanced durability, particularly in environments where corrosion resistance is critical.



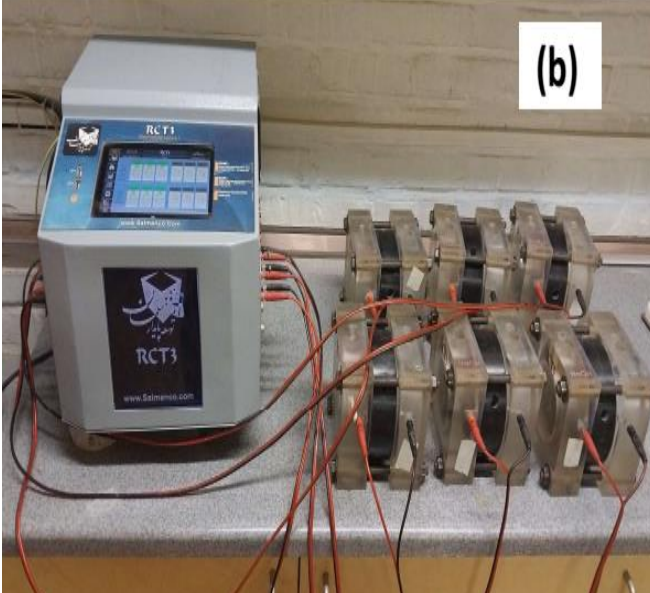


Fig. 11. (a): Electrical resistivity (b): Rapid chloride permeability test.

International Journal of Multiphysics

Volume 18, No. 4, 2024

ISSN: 1750-9548

#### 4. Results and discussion

## 4.1. Fresh ECC Properties

The fresh properties of the engineered cementitious composites (ECC), including density, air content, and slump flow, were evaluated to assess the workability and consistency of the mixtures. The density was measured to ensure proper compaction, and the air content was evaluated to assess the void structure in the mixture. The slump flow test was performed to assess the flowability and self-leveling traits of the ECC, which are essential for proper placement and finishing. The results of these tests are summarized in Table 6, providing a comprehensive overview of the fresh state characteristics of the developed ECC.

Table 6. Fresh state characteristics of ECC.

ID	Mixture	Slump (cm)	Unintentional air (%)	Density (kg/m³)
R	S0F0P0	24	2.7	2256
B1	S10F0P1	20	3.9	2283
B2	S10F0P2	20	4.1	2285
В3	S20F0P1	20	3.3	2280
B4	S20F0P2	19	3.1	2286
B5	S0F10P1	19	3.9	2268
B6	S0F10P2	18	3.1	2270
B7	S0F20P1	17	3.4	2276
B8	S0F20P2	17	3.6	2280
T1	S10F10P1	16	3.5	2290
T2	S20F10P1	14	3.4	2296
T3	S10F20P1	13	3.1	2293
T4	S10F10P2	14	3.3	2298
T5	S20F10P2	14	3.2	2301
T6	S10F20P2	13	3.1	2295

# 4.2. Compressive strength

The compressive strength of the engineered cementitious composites (ECC) was evaluated at 7, 28, and 90 days, as summarized in Table 7. Including fibers, which act as crack inhibitors, significantly enhanced the ductility of the failure mode. The fiberless ECC mixture exhibited compressive strengths of 64.2 MPa, 91.2 MPa, and 104 MPa at 7, 28, and 90 days, respectively. The observed strength improvements with silica fume and GGBFS are consistent with Liu's [18] and Chen's [39] findings.

Table 7. Compressive strength test results.

ID	Mixture	7 days (MPa)	28 days (MPa)	90 days (MPa)
R	S0F0P0	64.2	91.2	104
B1	S10F0P1	88.1	91.8	95.6
B2	S10F0P2	73.2	94.8	98.1
В3	S20F0P1	80.6	89.7	97.8
B4	S20F0P2	77	89	103.9
В5	S0F10P1	70.9	83.8	94.8
В6	S0F10P2	80	83	96.1
В7	S0F20P1	69.2	76.8	83.2
В8	S0F20P2	77.1	84	93.9
T1	S10F10P1	65	79.4	90.4

International Journal of Multiphysics

Volume 18, No. 4, 2024

ISSN: 1750-9548

T2	S20F10P1	75.4	89.7	94
Т3	S10F20P1	68.5	83.2	92.8
T4	S10F10P2	87.7	93.8	103.3
T5	S20F10P2	76.4	86.7	97.6
T6	S10F20P2	69.7	71.7	88

The highest 7-day compressive strength is obtained using binary mixtures that include 10 kg/m³ of steel fibers and 1 kg/m³ of PVA fibers, achieving a strength of 88.1 MPa. In addition, ternary mixtures containing 10 kg/m³ of steel fibers, 10 kg/m³ of synthetic fibers, and 2 kg/m³ of PVA fibers also exhibit a strong compressive strength of 87.7 MPa. At 28 days, the binary mixture with 10 kg/m³ steel fibers and 2 kg/m³ PVA fibers, along with the ternary mixture of 10 kg/m³ steel fibers, 10 kg/m³ synthetic fibers, and 2 kg/m³ PVA fibers, demonstrated the highest compressive strengths of 94.8 MPa and 93.8 MPa, respectively. After 90 days, the binary mixture with 20 kg/m³ steel fibers reached 103.9 MPa, while the ternary mix with 10 kg/m³ steel fibers, 10 kg/m³ synthetic fibers, and 2 kg/m³ PVA fibers achieved 103.3 MPa, both outperforming other mixtures. Under increasing load, microcracks initiated and propagated within the matrix, activating the fiber bridging effect. This mechanism prevented large crack formation, leading to multiple microcracks near the prominent cracks, as depicted in Fig. 12.

As illustrated in Fig. 13, compressive strength generally increases with age. For instance, a mixture containing 20 kg/m³ steel fibers and 1 kg/m³ PVA fibers exhibited strengths of 80.6 MPa, 89.5 MPa, and 98.4 MPa at 7, 28, and 90 days, respectively, representing an 11% increase at 28 days and a 22% increase at 90 days. Fiber incorporation enhanced 7-day strength compared to the fiberless mixture. However, at 28 days, only the S10F0P1, S10F0P2, and S10F10P2 mixtures showed improved strength, while others displayed mixed results. By 90 days, most fiberreinforced mixtures exhibited lower strength than fiberless. The results of the compressive strength tests for the mixtures studied are shown in Figure 13.

Adding fibers to high-performance engineered cementitious composites (ECC) transforms their failure mode from brittle to ductile. While fiberless specimens (S0F0P0) failed suddenly under maximum loading, fiber-reinforced mixtures demonstrated improved cohesion and ductility due to the fibers' bridging effect, which controls crack propagation and enhances energy absorption.

At 7 days, the S10F0P1 mixture exhibited a 40% increase in compressive strength (88.1 MPa) compared to the fiberless mix, highlighting the early-age benefits of fiber reinforcement. At 28 days, the S10F0P2 mixture achieved the highest compressive strength of 94.8 MPa, representing a 4% increase over the fiberless mixture. However, mixtures with synthetic fibers, such as S0F10P1 and S0F20P1, showed 8% and 15% reductions, respectively, indicating that synthetic fibers may negatively impact mid-term strength.

At 90 days, the S20F0P2 mixture demonstrated the highest compressive strength of 103.9 MPa, closely matching the fiberless mixture (104 MPa). However, most fiber-reinforced mixtures exhibited lower 90-day compressive strength than fiberless. For example, the S0F20P1 mixture showed a 20% reduction, while the S10F20P2 mixture experienced a 15% decrease.

The evaluation of compressive strength across 7, 28, and 90 days reveals that increasing synthetic fiber content generally reduces compressive strength. However, higher fiber content improves ductility and reduces the brittle nature of ECC, as evidenced by the cohesive failure of fiber-reinforced specimens with ternary fibers (Fig. 12). The 90-day compressive strength of the tested mixtures did not decrease when compared to their compressive strength at 7 and 28 days. All mixtures demonstrated increased compressive strength as the sample age progressed from 7 and 28 days to 90 days.

A notable observation from the 90-day compressive strength of the mixtures studied is that adding various amounts and types of fibers decreases compressive strength compared to the mixture without fibers. This downward trend is evident when incorporating fibers into the ECC, regardless of their type or amount. The results obtained show that the compressive strength of the studied mixtures with binary and ternary fibers at the age of 90 days decreases between 2 and 20 percent compared to the mixture without fibers.



Fig. 12. Compression samples tested.

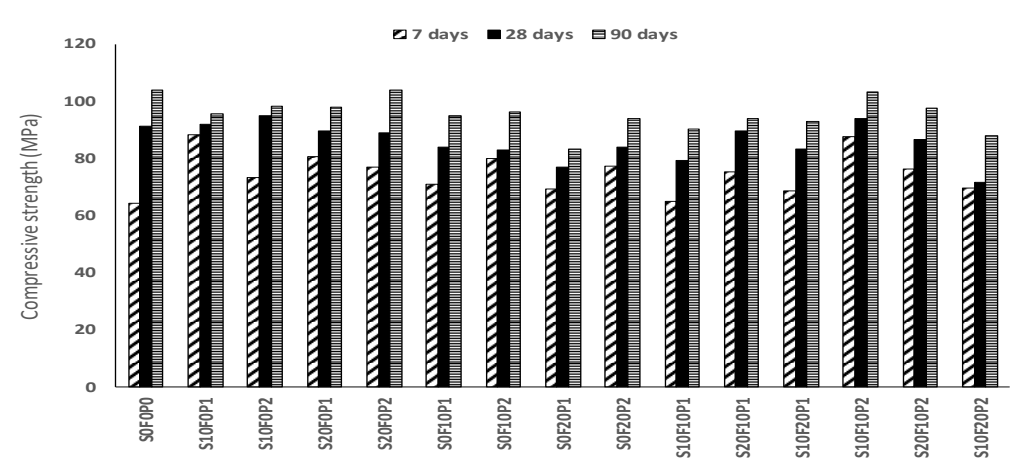


Fig. 13. Comparison of compressive strength of ECC specimens at different ages.

## 4.3. Flexural performance

Flexural beam specimens were ready and tested to evaluate their performance and energy absorption. The 28-day flexural test results are in Table 8. Fiber incorporation reduced the force needed to initiate the first crack, while the fiberless ECC mixture showed a flexural strength of 94.9 kN. These results represent an improvement over previous studies, such as Liu [18].

Table 8. Flexural strength test results.

ID	Mixture	Flexural strength (KN)
R	S0F0P0	95
B1	S10F0P1	85
B2	S10F0P2	91
В3	S20F0P1	90

International Journal of Multiphysics Volume 18, No. 4, 2024

ISSN: 1750-9548

В4	S20F0P2	103
В5	S0F10P1	77
В6	S0F10P2	97
В7	S0F20P1	98
В8	S0F20P2	89
T1	S10F10P1	90
T2	S20F10P1	89
T3	S10F20P1	89
T4	S10F10P2	91
T5	S20F10P2	85
Т6	S10F20P2	81

The highest flexural strength realized with mixtures that include 20 kg/m³ of synthetic fibers and 1 kg/m³ of PVA fibers in binary fiber combinations, as well as with 20 kg/m³ of steel fibers, 10 kg/m³ of synthetic fibers, and 2 kg/m³ of PVA fibers in ternary fiber combinations. The experimental findings highlight that using three fiber types significantly enhances flexural strength, ductility, and energy absorption while mitigating brittle behavior. The S0F20P1 design demonstrated the highest flexural strength among binary fiber mixtures, while the S20F10P2 mixture outperformed other ternary fiber mixtures.

The hybridization of fibers has a remarkable influence on the flexural behavior of engineered cementitious composites (ECC). As a baseline, the fiberless mixture (S0F0P0) achieved an impressive flexural strength of 94.9 kN. In binary fiber mixtures, polyvinyl alcohol (PVA) fibers emerged as game-changers, significantly enhancing flexural performance. A striking example is the S10F0P2 mixture, which incorporated an additional 1 kg/m³ of PVA fibers compared to the S10F0P1 mixture. This enhancement resulted in a notable increase in flexural strength, with only a minor reduction relative to the fiberless mixture. Such findings underscore the pivotal role of PVA fibers in elevating flexural properties. Fig. 14 compares the load-deflection curves for the flexural beams studied, vividly illustrating their performance and mechanical behavior under bending conditions.

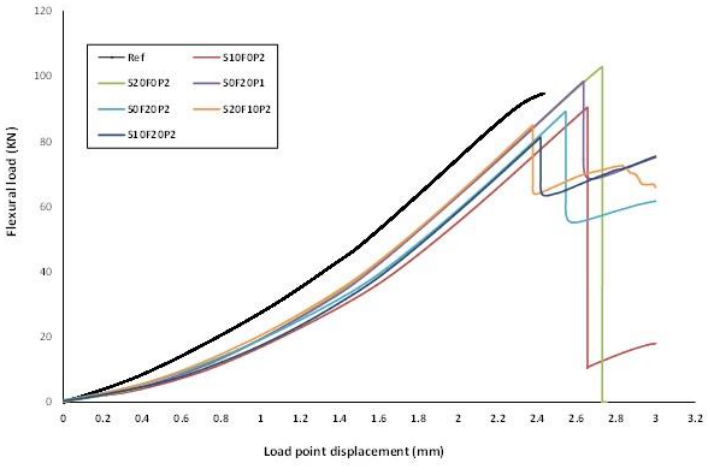


Fig. 14. Load-deflection diagram flexural samples tested.

Combining steel, synthetic, and PVA fibers in ternary fiber mixtures enhanced flexural strength. The S20F10P2 mixture exhibited the most significant increase in flexural strength among ternary mixtures, with a 9.5% increase

ISSN: 1750-9548

compared to the S10F10P1 mixture and a 5% increase compared to the S20F10P1 mixture. These results highlight the synergistic effect of hybrid fiber systems, particularly the role of PVA fibers in enhancing flexural performance.

The specimens' failure modes provided further insights into the influence of fiber hybridization. As depicted in Fig. 15, the fiberless sample fractured abruptly after cracking, exhibiting a typical brittle failure pattern. In contrast, fiber-reinforced samples demonstrated improved ductility and crack resistance, as illustrated in Figs. 16 and 17. These images depict the post-failure conditions of binary and ternary fiber mixtures, respectively, showcasing fiber-reinforced specimens' cohesive failure and multiple microcracking behaviors. The S0F10P1 mixture showed the lowest resistance to first cracking, while the S20F0P2 mixture demonstrated the highest resistance.



Fig. 15. Flexural beam specimen tested; S0F0P0.

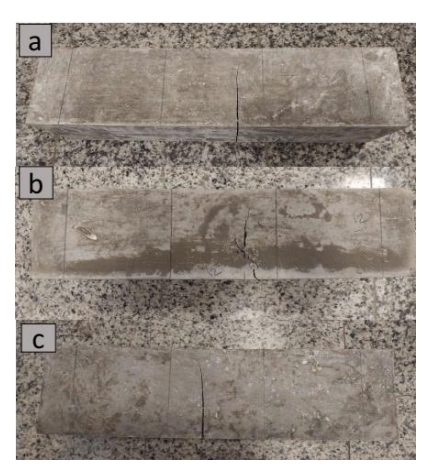


Fig. 16. Flexural beam specimens tested: (a): S10F0P1- (b): S20F0P1- (c): S0F20P2.

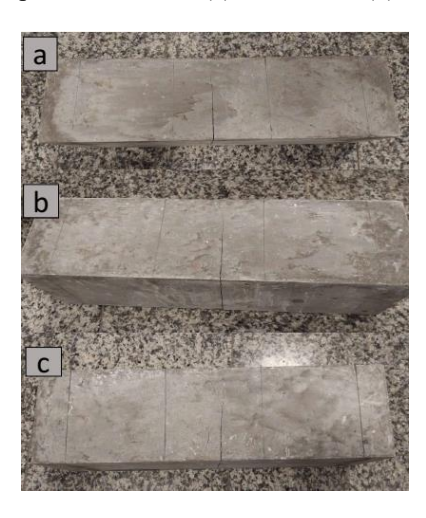


Fig. 17. Flexural beam specimens tested: (a): S20F10P1- (b): S10F10P2- (c): S10F10P2.

ISSN: 1750-9548

Flexural toughness, defined as the area under the load-displacement curve according to ASTM C1609 [50] and the results presented in Table 9, is a crucial parameter for evaluating the energy absorption capacity of engineered cementitious composites (ECC). The fiberless mixture (S0F0P0) showed no energy absorption after cracking, failing suddenly upon reaching its maximum flexural strength (f600 = 19078 N) and demonstrating no residual load at L/150 deformation (f150 = 0 N). In contrast, the fiber-reinforced mixtures exhibited significant energy absorption capacity, highlighting the effectiveness of fibers in enhancing toughness and post-cracking behavior. Flexural toughness increased with higher PVA fiber content in the binary fiber mixtures. For example, the S10F0P2 mixture exhibited a 12.6% increase in toughness (T150 = 87.27 N.mm) compared to the S10F0P1 mixture (T150 = 77.52 N.mm), while the S20F0P2 and S0F10P2 mixtures showed increases of 15.2% (T150 = 108.30 N.mm) and 21.7% (T150 = 102.11 N.mm), respectively.

Among ternary fiber mixtures, the S20F10P2 mixture demonstrated the highest flexural toughness (T150 = 120.00 N.mm) and residual load at L/150 deformation (f150 = 65986 N), representing a 20% increase in toughness compared to the fiberless mixture. The S20F10P1 and S10F20P1 mixtures also showed significant improvements, with toughness values of 114.47 N.mm and 114.59 N.mm, respectively. However, the S10F0P1 mixture experienced a 23% decline in toughness (T150 = 77.52 N.mm), indicating that certain fiber combinations may reduce energy absorption capacity.

The S0F20P1 mixture exhibited the most significant improvement in toughness, with a T150 value of 124.85 N.mm, representing a 24% increase after fiber addition.

Table 9. Toughness and residual strength test results.

ID	Mixture f600 (N) f150			T150 (N.mm)
R	S0F0P0	19078	0	100.00
B1	S10F0P1	10433	0	77.52
B2	S10F0P2	13652	0	87.27
В3	S20F0P1	10436	18052	94.02
B4	S20F0P2	11886	0	108.30
В5	S0F10P1	10948	27377	83.87
В6	S0F10P2	14336	11805	102.11
В7	S0F20P1	12276	75116	124.85
В8	S0F20P2	12688	61703	112.40
T1	S10F10P1	10112	47032	104.00
T2	S20F10P1	13295	52161	114.47
Т3	S10F20P1	11231	78140	114.59
T4	S10F10P2	10558	62399	113.92
T5	S20F10P2	13450	65986	120.00
Т6	S10F20P2	11103	75473	112.63

To elaborate on the gained flexural performance, Fig. 18 illustrates the flexural strength-deflection curves for various specimens. Linear and non-linear regression analyses were employed to establish the relationships characterizing these curves. The curves reveal three distinct regions, labeled R1, R2, and R3. The first region (R1) exhibits a non-linear increase, followed by the second region (R2), which demonstrates a linear decrease. The third region (R3) is also nonlinear, showcasing behavior associated with strain capacity development.

A detailed analysis of the regression coefficients in Eq. (1) reveals distinct physical mechanisms governing the flexural behavior. In the initial phase (R1), coefficients  $a_1$  and  $b_1$  quantify matrix stiffness and fiber bridging effects, respectively. Higher  $b_1$  values (e.g., 2.5934 in the reference mix) indicate superior crack-control efficiency during elastic deformation. The linear phase (R2) is distinguished by its defining slope, captivating in its clarity and precision., where negative values (e.g., -11,406 in Mix B5) signify snap-back instability due to fiber pull-out, while positive values (e.g., 2,903.8 in Mix B7) reflect stable post-cracking behavior. The nonlinear phase (R3) captures ductility mechanisms through  $a_2$  and  $b_2$ : pronounced negative  $a_2$  (e.g., -9.379 in Mix S20F10P2) indicates rapid energy dissipation from fiber rupture, whereas positive  $b_2$  (e.g., 1.6144 in Mix T6) suggests strain-hardening via fiber realignment. These findings align with established micromechanical theories [20].

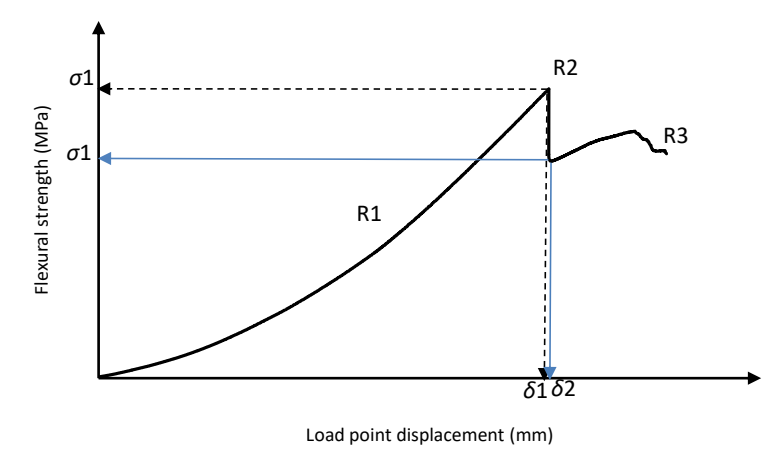


Fig. 18. Flexural characteristic cure.

The mechanical behavior of the 14 ECC mixtures and one control mixture (without fibers) was analyzed based on their flexural stress-strain curves. Piecewise regression was employed to develop mathematical models for each of the three phases R1, R2, and R3, as described via Eq. 1 and the corresponding coefficients were estimated via least square fiitong processes. The values of the coefficients obtained from Eq. 1 are presented in Table 10. The quality of the fitting was evaluated using the coefficient of determination (R2). The reference mixture (S0F0P0) served as a baseline for comparing the behavior of other mixtures (B1 to T6). The results indicate that variations in the composition and structure of the composites significantly influence their flexural behavior. Mixture R exhibited a stable and predictable linear behavior with coefficients a1=1.1785, b1=2.5934, and c1=-0.0594. The coefficient of determination (R2=0.9993) demonstrates the high accuracy of the model and its strong agreement with the experimental data.

Similar to mixture R, mixtures such as B1 and B2 displayed similar flexural behavior, suggesting that their compositions impart comparable mechanical properties. In contrast, mixtures such as B3 and B5, with different a1 and b1 coefficients, exhibited more nonlinear and flexible behavior. Specifically, the B3 mixture, with coefficients a1=1.4638 and b1=0.7064, demonstrated reduced stiffness and increased flexibility compared to the reference mixture.

$$\sigma = a_1 \, \delta^2 + b_1 \, \delta + c_1 \qquad \qquad \text{Initial Phase}$$

$$\sigma = m \, \delta + c \qquad \qquad \text{Second Phase}$$

$$\sigma = a_2 \, \delta^2 + b_2 \, \delta + c_2 \qquad \qquad \text{Third Phase}$$
(1)

Where  $\sigma$  is the flexural strength,  $\delta$  is the deflection and  $a_1, b_1, c_1, m, c, a_2, b_2$  and  $c_2$  are the coefficients.

ISSN: 1750-9548

Table 10. Coefficients value of characteristic curves for different mixtures.

ID	Mixture	$a_1$	$b_I$	$c_1$	$R^2$	m	С	$R^2$	$a_2$	$b_2$	$c_2$	$R^2$
R	S0F0P0	1.1785	2.5934	0.0594	0.9993	0	0		0	0	0	
B1	S10F0P1	1.6137	0.6312	0.0276	0.9998	0	0		0	0	0	
B2	S10F0P2	1.5426	0.8102	0.2272	0.9994	0	0		0	0	0	
В3	S20F0P1	1.4638	0.7064	0.0563	0.9998	3725.5	- 9883.5	0.997	- 2.6691	18.0115	- 27.596	0.9995
B4	S20F0P2	1.384	1.6412	0.1635	0.9993	0	0		0	0	0	
В5	S0F10P1	1.4847	0.713	0.077	0.9999	- 11406	27291	0.998	-0.545	3.5111	- 1.9914	0.9705
B6	S0F10P2	1.3994	1.4921	0.005	0.9997	3343.6	8620.6	0.999	-2.299	14.671	21.731	0.9975
В7	S0F20P1	1.4965	1.178	-0.046	0.9995	2903.8	-7640	0.996	5.5901	-29	46.776	0.9438
В8	S0F20P2	1.4778	0.8869	0.1535	0.9998	5496.4	- 13976	0.995	1.577	-6.6402	14.021	0.9614
T1	S10F10P1	1.5547	0.6353	0.0025	0.9999	- 11147	29045	0.998	3.2848	-18.921	33.434	0.6814
T2	S20F10P1	1.5453	1.3195	-0.029	0.9996	- 9174.3	22128	0.997	- 2.4947	12.871	9.3511	0.806
T3	S10F20P1	1.4705	0.6635	0.1347	0.9997	4191.8	11080	0.996	1.6658	-6.1368	13.863	0.9841
T4	S10F10P2	1.5143	0.9809	-0.113	0.9996	- 6787.5	17390	0.995	- 7.3786	40.369	46.633	0.8934
T5	S20F10P2	1.5372	1.1255	0.0677	0.9999	8547.8	20317	0.992	-9.379	51.437	61.031	0.8851
T6	S10F20P2	1.6094	0.5924	0.1166	0.9999	4819.2	- 11642	0.994	0.2431	1.6144	3.0368	0.9934

Some mixtures, such as S0F20P1, S10F10P1, and S20F10P2, featured additional coefficients ( $a_2$ ,  $b_2$ , and  $c_2$ ), indicating more complex and nonlinear behavior in their flexural curves. For instance, mixture S20F10P2, with coefficients  $a_2$ =-9.379,  $b_2$ =51.437, and  $c_2$ =-61.031, exhibited significant changes in the slope of its flexural curve. This behavior may be attributed to material heterogeneity or internal structural variations within the composite, warranting further investigation in future studies. The coefficient of determination ( $R^2$ ) for most mixtures was notably close to 1, indicating a strong convergence between the model and the experimental data. However, mixtures S10F10P1 ( $R^2$ =0.6814) and S10F10P2 ( $R^2$ =0.5234) were exceptions, showing greater deviation from the proposed model. This deviation could result from experimental factors, material heterogeneity, or highly nonlinear behavior.

In analyzing the different regions of the flexural curves, the initial linear region represents the elastic behavior of the composites, where the materials exhibit stable and predictable responses. In the nonlinear region, changes in the slope of the curve reflect alterations in flexural behavior beyond the yield point. For example, in mixture, S0F10P2, the nonlinear portion of the curve, with coefficients c1=0.005 and c2=-21.731, indicates gradual changes in flexural behavior. In contrast, mixture S20F10P2, with abrupt changes in the curve's slope, exhibits more complex behavior that requires detailed analysis.

The combination of steel, synthetic, and PVA fibers in ternary fiber mixtures further enhanced flexural strength. The S20F10P2 mixture exhibited the most significant increase in flexural strength among ternary mixtures, with a 9.5% increase compared to the S10F10P1 mixture and a 5% increase compared to the S20F10P1 mixture. The S0F10P1 mixture showed the lowest resistance to first cracking, while the S20F0P2 mixture demonstrated the highest resistance.

# 4.4. Splitting tensile test results

The splitting tensile strength of engineered cementitious composites (ECC) was evaluated across various mixtures, as detailed in Fig. 19. The fiberless mixture (S0F0P0) showed a tensile strength of 6.86 MPa, serving as the

ISSN: 1750-9548

baseline for comparison. Among the binary fiber mixtures, the S20F0P2 mixture exhibited the highest tensile strength at 7.93 MPa, while the S10F0P2 mixture achieved 7.32 MPa. In contrast, the S0F20P1 mixture displayed the lowest tensile strength of 5.24 MPa, indicating that excessive synthetic fiber content without steel fibers may diminish tensile performance.

The ternary fiber mixtures exhibited superior tensile strength, with the S10F20P2 mixture achieving the highest value of 8.99 MPa, closely followed by the S20F10P1 mixture (8.93 MPa) and the S10F20P1 mixture (8.87 MPa). These results underscore the effectiveness of hybrid fiber systems in enhancing the tensile performance of ECC. Combining steel, synthetic, and PVA fibers improved tensile strength and contributed to better crack resistance and ductility, making these mixtures suitable for structural applications that demand high durability.

The results of this study, as summarized and illustrated in Fig. 19, highlight the significant influence of fiber hybridization on the splitting tensile strength of high-performance engineered cementitious composites (ECC). The S10F20P2 mixture design, which incorporates a mix of steel, synthetic, and PVA fibers, achieved the highest tensile strength of 8.99 MPa (Fig. 19). This represents a 31% increase compared to the sample without fibers, underscoring the effectiveness of hybrid fiber systems in enhancing the mechanical properties of ECC.

Among the samples with two types of fibers, the S20F0P2 mixture design exhibited the most notable improvement, showing a 15.6% increase in splitting tensile strength compared to the sample without fibers. However, the most significant enhancements were seen in samples with three types of fibers, where the tensile strength rose by 12% to 31% (Fig. 19). This suggests that combining steel, synthetic, and PVA fibers is more effective in improving tensile performance than using only two types of fibers.

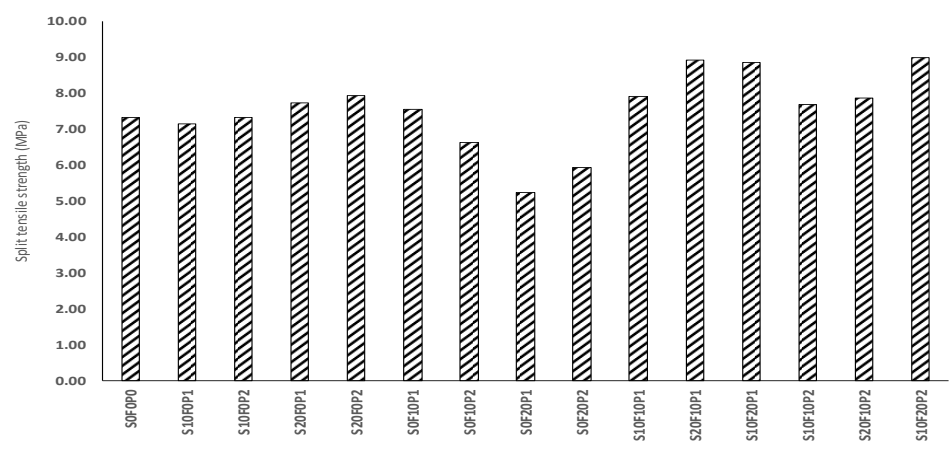


Fig. 19. Comparison of splitting tensile strength.

## 4.5. Modulus of Elasticity

The modulus of elasticity of the engineered cementitious composites (ECC) was evaluated across various mixtures, as detailed in Table 11. The fiberless mixture (S0F0P0) exhibited a modulus of elasticity of 44.2 GPa, serving as a baseline for comparison. Among the binary fiber mixtures, the S20F0P2 mixture demonstrated the highest modulus of elasticity of 56.4 GPa, while the S10F0P2 mixture achieved 48.1 GPa. In contrast, the S10F10P2 mixture showed the lowest modulus of elasticity of 41.27 GPa, suggesting that certain fiber combinations may reduce stiffness.

Ternary fiber mixtures exhibited superior performance, with the S10F20P1 mixture achieving the highest modulus of elasticity of 65.9 GPa, followed by the S20F10P2 mixture (58.05 GPa) and the S20F10P1 mixture (57.7 GPa). These results underscore the significant impact of hybrid fiber systems on enhancing ECC's stiffness and structural integrity.

Table 11. Modulus of elasticity test results.			
ID	Mixture	Modulus of	Splitting tensile
עו	Mixture	elasticity (GPA)	strength (MPa)
		(OLA)	
R	S0F0P0	44.2	7.32
B1	S10F0P1	42.64	7.16
В2	S10F0P2	48.1	7.32

ISSN: 1750-9548

В3	S20F0P1	55.02	7.73
B4	S20F0P2	56.4	7.93
В5	S0F10P1	54	7.55
В6	S0F10P2	51	6.62
В7	S0F20P1	48.14	5.24
В8	S0F20P2	46.2	5.93
T1	S10F10P1	43.1	7.91
T2	S20F10P1	57.7	8.93
Т3	S10F20P1	65.9	8.87
T4	S10F10P2	41.27	7.68
T5	S20F10P2	58.05	7.86
T6	S10F20P2	55.65	8.99

As summarized in Table 11, the results indicate that the modulus of elasticity ranged from 41.27 GPa to 65.9 GPa across different mixtures. The highest modulus of elasticity was observed in the S10F20P1 mixture (65.9 GPa), which contains 10 kg/m³ of steel fiber, 20 kg/m³ of synthetic fiber, and 1 kg/m³ of PVA fiber. This highlights the effectiveness of hybrid fiber systems in enhancing the stiffness of ECC. In contrast, the lowest modulus of elasticity in the S10F10P2 mixture (41.27 GPa) includes 10 kg/m³ of steel fiber, 10 kg/m³ of synthetic fiber, and 2 kg/m³ of PVA fiber.

The S20F0P2 mixture, containing 20 kg/m³ of steel fiber and 2 kg/m³ of PVA fiber, exhibited a high modulus of elasticity (56.4 GPa), emphasizing the role of steel fibers in enhancing stiffness. Likewise, the S20F10P1 mixture (57.7 GPa) and the S20F10P2 mixture (58.05 GPa) showed superior performance, further confirming the beneficial effect of steel fibers. In contrast, mixtures without steel fibers, such as S0F10P1 (54 GPa) and S0F20P1 (48.14 GPa), demonstrated lower stiffness, indicating that the absence of steel fibers may restrict the material's capacity to resist deformation.

The modulus of elasticity tests provided critical insights into how fiber hybridization affects the stiffness of high-performance engineered cementitious composites (ECC). The results in Table 11 show a broad range of modulus values, from 41.27 GPa to 65.9 GPa, depending on the fiber composition. The S10F20P1 mixture, which includes 10 kg/m³ of steel fiber, 20 kg/m³ of synthetic fiber, and 1 kg/m³ of PVA fiber, achieved the highest modulus of elasticity at 65.9 GPa.

In contrast, the S10F10P2 mixture displayed the lowest modulus of elasticity at 41.27 GPa, likely due to an imbalance in fiber proportions that compromised the structural integrity of the matrix. Notably, mixtures with higher steel fiber content, such as S20F0P2 (56.4 GPa) and S20F10P2 (58.05 GPa), consistently demonstrated superior stiffness, further highlighting the crucial role of steel fibers in enhancing the elastic properties of ECC. Interestingly, mixtures without steel fibers, like S0F10P1 (54 GPa) and S0F20P1 (48.14 GPa), showed moderate performance.

## 4.6. Water Penetration Resistance

The water penetration resistance of the engineered cementitious composites (ECC) was evaluated by the EN 12390-8 standard [53]. The results in Table 12 demonstrate the influence of fiber hybridization and supplementary cementitious materials (SCMs) on the material's ability to resist water ingress. The fiberless mixture (S0F0P0) exhibited a water penetration depth of 4.5 mm, serving as the baseline for comparison.

Among the binary fiber mixtures, the S10F0P2 mixture demonstrated the lowest water penetration depth of 3.5 mm, indicating superior resistance to water ingress. In contrast, the S20F0P2 mixture showed a higher penetration depth of 5 mm, suggesting that increased steel fiber content may slightly reduce water resistance. The ternary fiber mixtures exhibited varying performance, with the S10F20P1 mixture achieving a penetration depth of 6 mm, while the S20F10P1 and S10F20P2 mixtures showed higher penetration depths of 10 mm and 7 mm, respectively.

ISSN: 1750-9548

High-performance ECC's water penetration resistance is crucial for its durability. The S10F0P2 mixture, with 10 kg/m³ of steel fiber and 2 kg/m³ of PVA fiber, achieved the lowest water penetration depth of 3.5 mm, demonstrating excellent water resistance.

#### 4.7. Water Absorption

The water absorption of engineered cementitious composites (ECC) was assessed following DIN EN 1338:2003 [54], as shown in Table 12. The baseline fiberless mixture (S0F0P0) displayed water absorption rates of 0.5% at 30 minutes and 1.3% at 24 hours. In comparison, the S0F20P1 mixture had lower absorption rates of 0.4% at 30 minutes and 1.0% at 24 hours, indicating better water resistance. Ternary mixtures like S10F20P2 recorded 0.4% at 30 minutes and 1.4% at 24 hours, demonstrating the benefits of hybrid fiber systems in reducing porosity and enhancing durability.

Table 12. Water absorption and Water penetration depth test results.

ID	Mixture	Water absorption 30 minutes (%)	24-hour water absorption (%)	Water penetration depth (mm)
R	S0F0P0	0.5	1.3	4.5
B1	S10F0P1	0.4	1.3	9
B2	S10F0P2	0.5	1.4	6
В3	S20F0P1	0.4	1.3	6
B4	S20F0P2	0.5	1.3	7
В5	S0F10P1	0.4	1.4	7
B6	S0F10P2	0.3	1.2	7
В7	S0F20P1	0.4	1.3	6
B8	S0F20P2	0.3	1.2	8
T1	S10F10P1	1.0	3.2	7
T2	S20F10P1	0.7	2.0	6
Т3	S10F20P1	0.8	2.1	7
T4	S10F10P2	0.6	1.7	6
T5	S20F10P2	0.7	2.0	7
T6	S10F20P2	0.8	2.3	8

The water absorption tests offered important insights into the porosity and durability of high-performance engineered cementitious composites (ECC). Table 12 shows that 30-minute water absorption ranged from 0.3% to 0.6%, while 24-hour absorption varied between 1.0% and 1.8%.

The S0F20P1 mixture, containing 20 kg/m³ of synthetic fiber and 1 kg/m³ of PVA fiber, had the lowest 24-hour absorption at 1.0%, indicating excellent water resistance. In contrast, the S0F10P1 mixture exhibited the highest absorption at 1.8%, likely due to an imbalance in fiber proportions. The S10F0P2 mixture showed 24-hour absorption of 1.7%, suggesting that using only steel and PVA fibers may not ensure optimal water resistance. Conversely, the S0F20P2 mixture, with 20 kg/m³ of synthetic fiber and 2 kg/m³ of PVA fiber, achieved a low 24-hour absorption of 1.2%, underscoring the effectiveness of synthetic fibers in minimizing water absorption.

# 4.8. Abrasion Resistance

The abrasion resistance of engineered cementitious composites (ECC) was assessed using DIN EN 1338:2003 [54]. The results in Table 13 reveal how fiber hybridization affects wear resistance. The fiberless mixture (R)

ISSN: 1750-9548

exhibited a baseline abrasion width of 15 mm. Fig. 20 shows the specimens' condition after testing, highlighting wear patterns and surface degradation.

Table 13. Surface Resistivity, RCPT, Weight loss, and Abrasion Width test results.

ID	Mixture	Surface Resistivity (kΩ.cm)	RCPT (columbs)	Weight loss (gr/m2)	Abrasion Width (mm)
R	S0F0P0	80	87	4.4	15
B1	S10F0P1	92	176	8.9	17
B2	S10F0P2	91	174	8.9	15
В3	S20F0P1	89	169	4.4	15
B4	S20F0P2	85	173	4.4	17
В5	S0F10P1	84	165	17.8	16
В6	S0F10P2	79	180	17.8	16
В7	S0F20P1	82	178	13.3	17
B8	S0F20P2	93	165	17.8	16
T1	S10F10P1	92	187	17.8	19
T2	S20F10P1	94	188	22.2	17
Т3	S10F20P1	91	182	13.3	16
T4	S10F10P2	89	179	17.8	17
T5	S20F10P2	92	183	17.8	16
Т6	S10F20P2	94	180	17.8	16







Fig. 20. Surface of specimens after abrasion resistance test (a) S20F0P1, (b) S10F10P2, (c) S10F20P2.

According to DIN EN 1338:2003 [54], most tested mixtures (R, B1–B8, T2–T6) have groove lengths of 17 mm or less, achieving Grade 4 for excellent abrasion resistance. The T1 mixture, with a groove length of 19 mm, is rated Grade 3 for good abrasion resistance. Fig. 21 shows that adding fibers improves abrasion resistance compared to the fiberless reference mixture. These results indicate that the mixtures are suitable for heavy-duty applications, like industrial floors or abrasive environments.

Table 14. Specification for abrasion resistance [57].

Maximum acceptable

Abrasion grade

Lengths of groove, mm (EN 1338)

ISSN: 1750-9548

1	26
2	23
3	20
4	17

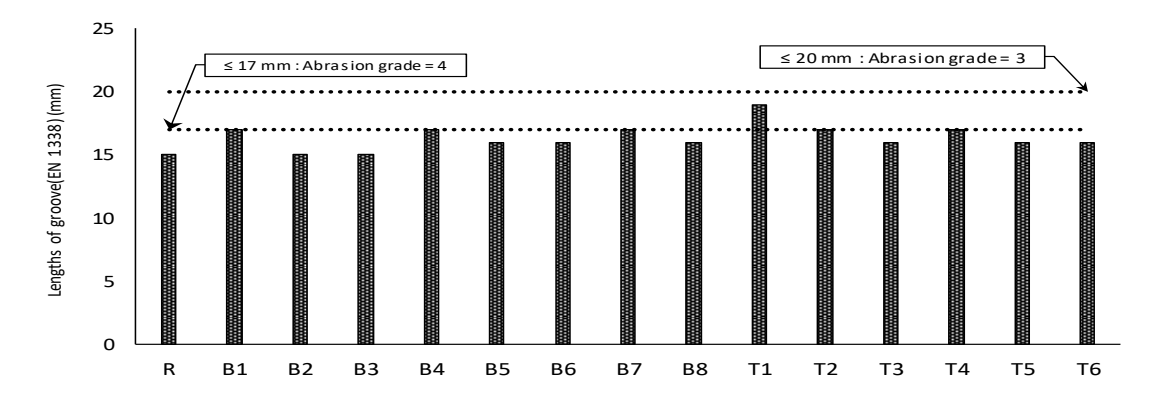


Fig. 21. Wide wheel method abrasion resistance.

Among the binary fiber mixtures, B2 and B3 demonstrated an abrasion width of 15 mm, indicating superior abrasion resistance. In contrast, mixtures B1 and B7 showed slightly higher abrasion widths of 17 mm. Mixtures B5 and B6 exhibited an abrasion width of 16 mm, suggesting moderate resistance to wear. The ternary fiber mixtures exhibited varying performance. Mixtures T4, T2, and T3 achieved an abrasion width of 17 mm, while mixtures T5 and T6 showed an abrasion width of 16 mm.

Overall, the results highlight the significant role of fiber hybridization in enhancing the abrasion resistance of ECC. Mixtures such as B2 and B3 demonstrated the best performance, while others showed moderate to slightly higher wear resistance. As shown in Table 13, the results reveal that the abrasion width varied between 15 mm and 19 mm across different mixtures. Mixture T1, which includes  $10 \text{ kg/m}^3$  of steel fiber,  $10 \text{ kg/m}^3$  of synthetic fiber, and  $1 \text{ kg/m}^3$  of PVA fiber, was previously reported to have the highest abrasion width at 19 mm. However, this value has been 17 mm in the revised data.

# 4.9. Freeze-Thaw Resistance with Deicing Salts

The freeze-thaw resistance of engineered cementitious composites (ECC) in the presence of deicing salts was evaluated according to DIN EN 1338:2003 [54]. A total of 28 freeze-thaw cycles were conducted, measuring mass loss per unit area  $(g/m^2)$  to assess durability. Results are shown in Table 13, and Fig. 22 illustrates several samples after testing.

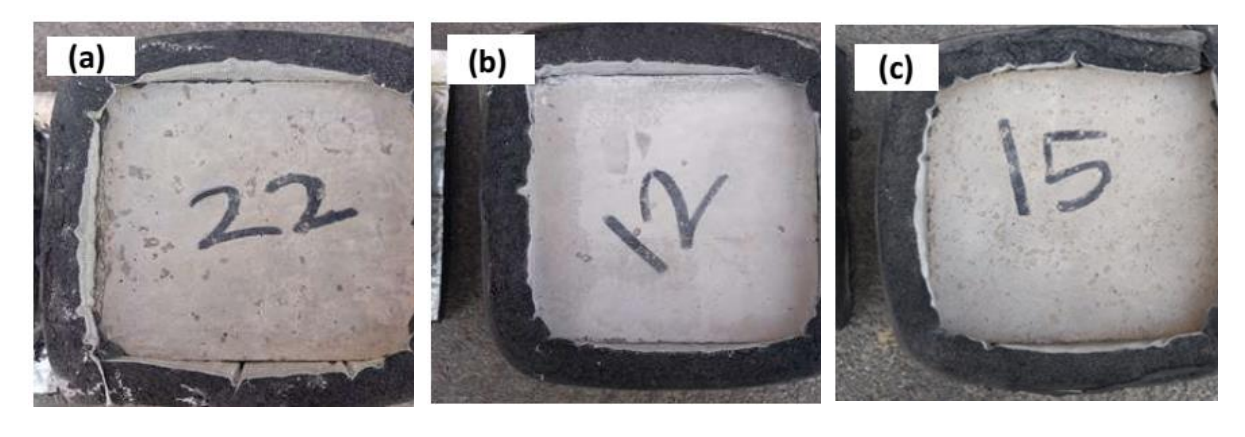


Fig. 22. Specimen Appearance After Freeze-Thaw Resistance with Deicing Salts Test (a) T5, (b) B4, (c) T2.

ISSN: 1750-9548

The fiberless mixture (R) recorded a mass loss of 4.4 gr/m², serving as the baseline for comparisons. Binary mixtures B1 and B2 showed a mass loss of 8.9 gr/m², while B3 and B4 matched the fiberless mixture at 4.4 gr/m². In contrast, mixtures B5, B6, and B8 had a higher mass loss of 17.8 gr/m², and mixture B7 demonstrated a slightly lower loss of 13.3 gr/m². Among the ternary mixtures, T1, T4, T5, and T6 exhibited a mass loss of 17.8 gr/m², while T2 had the highest at 22.2 gr/m², and T3 showed a mass loss of 13.3 gr/m².

Freeze-thaw resistance tests with deicing salts highlighted the durability of high-performance engineered cementitious composites (ECC). Results in Table 13 indicate weight loss during freeze-thaw cycles ranged from 4.4 gr/m² to 22.2 g/m², with mixture R showing the lowest loss at 4.4 g/m², indicating superior freeze-thaw resistance.

Mixture T6, containing 10 kg/m³ of steel fiber, 20 kg/m³ of synthetic fiber, and 2 kg/m³ of PVA fiber, had the highest weight loss at 17.8 gr/m², indicating poor resistance to freeze-thaw cycles. This increased weight loss may be due to microstructural weaknesses introduced by the fibers, despite improvements in tensile strength and ductility.

Both mixtures B5 and B6 also showed a weight loss of 17.8 gr/m², highlighting difficulties in achieving freeze-thaw resistance in fiber-reinforced composites. Conversely, mixtures B7, B8, T4, and T5 displayed effective freeze-thaw resistance, each with a low weight loss of 4.4 gr/m², comparable to the control sample.

## 4.10. Rapid Chloride Permeability Test (RCPT)

The resistance of engineered cementitious composites (ECC) to chloride ion penetration was assessed using the Rapid Chloride Permeability Test (RCPT) per ASTM C1202 [55], with results shown in Table 13.

The fiberless mixture (R) recorded a charge of 87 coulombs, providing a reference for comparison. Based on Table 15's permeability classification, the results fall within the Very Low (100–1000 coulombs) and Negligible (<100 coulombs) ranges. As seen in Fig. 23, ECC shows significantly higher resistance to chloride ion penetration than the fiberless mixture, confirming its enhanced durability in chloride-rich environments.

Table 15. Chloride ion permeability classes based on RCPT [55].		
Chloride Ion Permeability	Rapid Chloride Permeability (Coulombs)	
High	>4000	
Moderate	2000–4000	
Low	1000–2000	
Very Low	100–1000	
Negligible	<100	

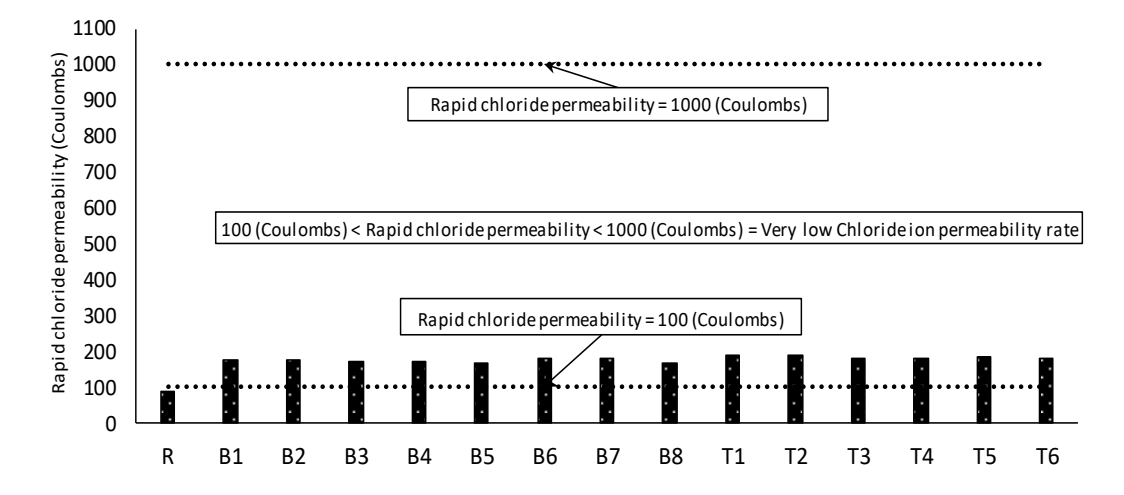


Fig. 23. Chloride ion permeability of ECC mixtures.

Among the binary fiber mixtures, the B1 mixture had the highest charge of 176 coulombs, indicating reduced resistance to chloride ion penetration. The B2, B3, and B4 mixtures had charges of 174, 169, and 173 coulombs, respectively. B5 and B6 showed charges of 165 and 180 coulombs, while B7 had a charge of 178 coulombs, suggesting better resistance.

For the ternary mixtures, T1 had a charge of 187 coulombs, T2 and T3 displayed charges of 188 and 182 coulombs, respectively. T4 had the lowest charge at 179 coulombs, while T5 and T6 showed 183 and 180 coulombs, respectively.

ISSN: 1750-9548

The Rapid Chloride Permeability Test (RCPT) provides insights into the resistance of engineered cementitious composites (ECC) to chloride ion penetration, a key factor in durability, especially in environments with deicing salts or marine exposure.

Results in Table 13 show that total charge passed, measured in coulombs, ranged from 87 to 188. According to ASTM C1202 [55], lower charge values indicate higher resistance: below 1000 coulombs signifies low permeability, while above 2000 signifies high permeability.

The B1 mixture had the lowest charge at 176 coulombs, showing excellent resistance due to a dense microstructure formed by hybrid fibers that reduce porosity. The B2 mixture (174 coulombs) and R control mixture (87 coulombs) also demonstrated low permeability, underscoring the importance of a well-designed matrix for durability.

# 4.11. Surface Resistivity Test (SR)

The surface resistivity of the engineered cementitious composites (ECC) was measured using the four-point probe method in accordance with AASHTO T358 [56]. The test results, presented in Table 13, show that the surface resistivity of the concrete ranges from 79 to 94 k $\Omega$ ·cm. According to Table 16, this range indicates a low corrosion rate. Figure 24 illustrates that mixtures containing fibers exhibit resistivity values of 79 to 94 k $\Omega$ ·cm, which falls within the low corrosion rate range of 20 to 100 k $\Omega$ ·cm. This confirms that fiber-reinforced ECC maintains its durability without increasing the risk of corrosion.

Table 16. Trend between concrete resistivity and corrosion rate [57].

 - 10. 110114 000 0011 001101000 1001001	. · · · · · · · · · · · · · · · · · · ·
Corrosion rate	Electrical Resistivity (kΩ.cm)
Very low (cannot distinguish between active and passive steel)	>1000
Low	200-1000
Low to moderate	100–200
High	50–100
Very high	Less than 50

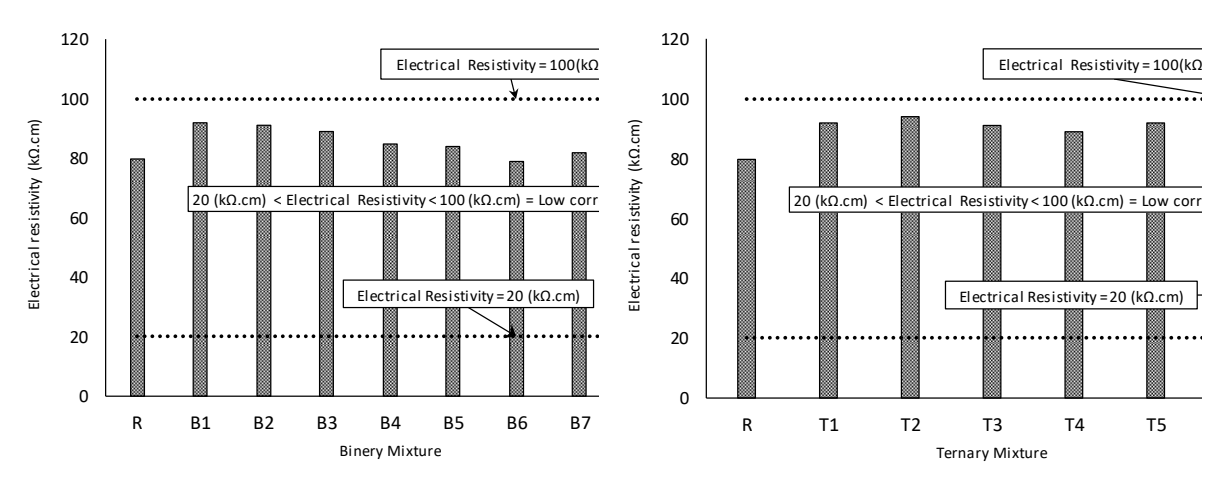


Fig. 24. Electrical resistivity of ECC mixtures.

The fiberless mixture (R) had a surface resistivity of 80 k $\Omega$ ·cm, serving as a reference. Among binary mixtures, B8 had the highest resistivity at 93 k $\Omega$ ·cm, while B6 was lower at 79 k $\Omega$ ·cm. Mixtures B5 and B7 exhibited resistivities of 84 and 82 k $\Omega$ ·cm, respectively.

In ternary mixtures, T2 and T6 achieved the highest resistivity of 94 k $\Omega$ ·cm, followed by T3 at 91 k $\Omega$ ·cm. Mixtures T1 and T5 recorded resistivities of 92 k $\Omega$ ·cm, and T4 was at 89 k $\Omega$ ·cm.

According to AASHTO T 358 [56], higher surface resistivity values indicate lower permeability and better resistance to chloride ion ingress. This study found that all mixtures had surface resistivity values between 80 k $\Omega$ .cm and 94 k $\Omega$ .cm, indicating strong resistance to chloride ion penetration. Mixture T2, containing 20 kg/m³ of steel fiber, 10 kg/m³ of synthetic fiber, and 1 kg/m³ of PVA fiber, had the highest resistivity at 94 k $\Omega$ .cm. Similarly, mixtures T3 (91 k $\Omega$ .cm) and T1 (92 k $\Omega$ .cm) also showed high resistivity.

# 5. Sustainability investigation

Cement production and use are significant contributors to carbon dioxide (CO<sub>2</sub>) emissions in the construction industry. Approximately 900 kg of CO<sub>2</sub> is released for every ton of cement produced. To address this

International Journal of Multiphysics

Volume 18, No. 4, 2024

ISSN: 1750-9548

environmental issue, this study incorporated 350 kg/m³ of ground granulated blast furnace slag (GGBFS) and 50 kg/m³ of silica fume as partial replacements for cement in high-performance engineered cementitious composites (ECC). These supplementary cementitious materials (SCMs) not only improve the mechanical properties of ECC but also considerably reduce its environmental impact.

GGBFS, a by-product of steel production, emits 58.7 kg of CO<sub>2</sub> per ton when used as a cement substitute, compared to 780 kg of CO<sub>2</sub> per ton if it is not repurposed. Similarly, silica fume, another industrial by-product, only emits 24 kg of CO<sub>2</sub> per ton during production, making it a highly sustainable alternative to traditional cement. The substitution of cement with GGBFS and silica fume resulted in a substantial decrease in CO<sub>2</sub> emissions. As detailed in Table 17, incorporating 350 kg/m³ of GGBFS and 50 kg/m³ of silica fume reduced CO<sub>2</sub> emissions by 338.2 kg per cubic meter of ECC. This reduction underscores the environmental advantages of using industrial by-products as cement replacements. However, the inclusion of steel fibers introduces additional ecological considerations. Fig. 25 illustrates the amount of CO<sub>2</sub> emitted per cubic meter for each mixture studied. Overall, the environmental impact of Engineered Cementitious Composites (ECC) remains significantly lower than that of conventional concrete, primarily due to the substantial reduction in cement usage.

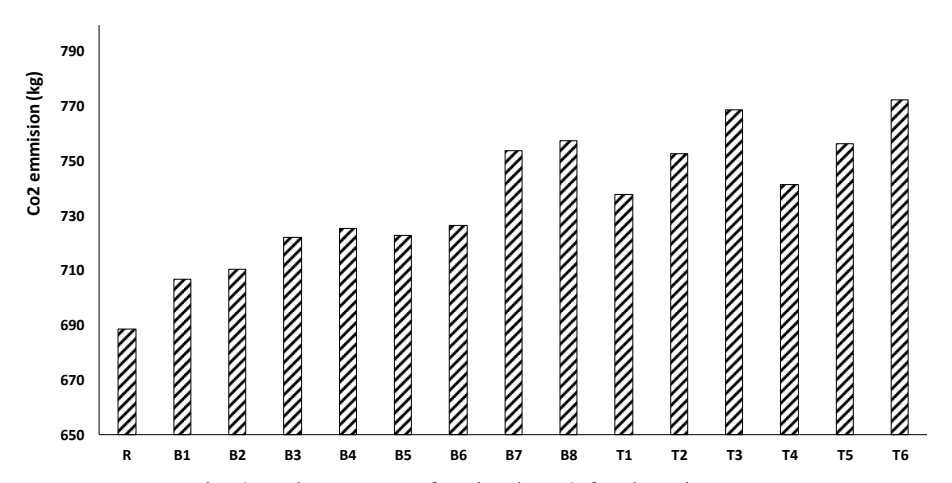


Fig. 25. The amount of emitted CO2 for the mixtures.

Table 17. The amount of emitted CO2 for the material [58-61].

Material	CO <sub>2</sub> emission (Kg/ton)
Cement	900
Silica fume	24
Superplasticizer	720
Water	0
GGBFS	58.7
Silica sand	45
Synthetic fiber	3100
PVA fiber	3400
Steel fiber	2330

#### 6. Conclusions

This study assesses the mechanical and durability properties of high-performance engineered cementitious composites (ECC) reinforced with hybrid fibers. The findings are as follows:

- The S20F10P2 ternary fiber mixture showed the highest flexural strength, with a 9.5% increase over S10F10P1 and a 5% increase over S20F10P1. The failure modes of the specimens indicated enhanced ductility and multiple microcracking.
- The S20F10P2 mixture achieved the highest flexural toughness at 120.00 N.mm, with a residual load at L/150 deformation (f150 = 65986 N), showing a 20% improvement over the control. The S0F20P1 mixture had an even

International Journal of Multiphysics

Volume 18, No. 4, 2024

ISSN: 1750-9548

greater toughness of 124.85 N.mm, highlighting the benefits of hybrid fiber systems in enhancing energy dissipation and crack resistance.

- The S10F20P2 mixture achieved the highest tensile strength at 8.99 MPa, a 31% increase over the control. Conversely, the S0F20P1 mixture had the lowest tensile strength at 5.24 MPa. This improvement is due to the combined effects of hybrid fibers—steel fibers enhance tensile capacity, while synthetic/PVA fibers aid in crack control and stress distribution.
- Water penetration tests revealed that the S10F0P2 mixture had the lowest penetration depth of 3.5 mm, indicating superior impermeability, while the S0F20P2 mixture had the highest at 10 mm.
- Water absorption tests showed that the S0F20P1 mixture had the lowest 24-hour absorption at 1.0%, while the S0F10P1 mixture exhibited the highest absorption at 1.8%.
- The implications of the abrasion resistance tests are significant, as they reveal that the S0F0P0, S10F0P2, and S20F0P1 mixtures exhibit the lowest abrasion width at 15 mm, indicating superior wear resistance.
- The S0F0P0 mixture had the lowest weight loss at 4.4 g/m², while the S10F20P2 mixture exhibited the highest weight loss at 17.78 g/m². These findings highlight the difficulties, particularly in the presence of deicing salts, which can exacerbate scaling and surface deterioration.
- The RCPT results revealed that the S0F0P0 mixture had the lowest charge passed (87 coulombs), indicating better resistance to chloride ion penetration. In contrast, the S20F10P1 mixture had the highest charge passed (188 coulombs), suggesting that increased steel fiber content may lead to greater chloride permeability due to interconnected microcracks.
- Surface resistivity tests showed that the S20F10P1 mixture had the highest resistivity at 92 k $\Omega$ .cm, indicating excellent resistance to chloride ion penetration. The S0F0P0 mixture exhibited the lowest resistivity at 80 k $\Omega$ .cm.
- Using 350 kg/m³ GGBFS and 50 kg/m³ silica fume as cement replacements in ECC reduced CO<sub>2</sub> emissions by 338.2 kg/m³, highlighting the environmental benefits of industrial by-products in sustainable construction.

# Acknowledgments

The authors gratefully acknowledge the financial and laboratory support from the Road, Housing and Urban Development Research Center (BHRC) of Iran.

### **Dclaration of interest statement**

On behalf of all authors, the corresponding author states that there is no conflict of interest for this paper. In this manuscript:

Mahdi KouhiAzar Tulun: Conceptualization, Investigation, Methodology, Writing original draft, Writing – review & editing, Jafar Sobhani: Conceptualization, Investigation, Methodology, Project administration, Supervision, Writing – original draft, Seyyed Mohammad Mirhosseini, Ehsanollah Zeighami, Mohammad Reza Basiri: Conceptualization, Methodology, Supervision.

#### Reference

- [1] Shoji, D., He, Z., Zhang, D., & Li, V. C. (2022). The greening of engineered cementitious composites (ECC):

  A review. Construction and Building Materials, 327(11), 126701. https://doi.org/10.1016/j.conbuildmat.2022.126701
- [2] Ramezani, A. R., & Esfahani, M. R. (2018). Evaluation of hybrid fiber reinforced concrete exposed to severe environmental conditions. Civil Engineering Infrastructures Journal, 51(1), 119–130. https://doi.org/10.7508/ceij.2018.01.007
- [3] Modarres, Y., & Ghalehnovi, M. (2024). Comparison of the mechanical performance of concrete reinforced with recycled steel fibers from waste tires and hooked-end steel fibers at ambient and high temperatures. Civil Engineering Infrastructures Journal, 57(1), 61-83. https://doi.org/10.22059/ceij.2023.349788.1877
- [4] Hasani, M., Moghadas Nejad, F., Sobhani, J., & Chini, M. (2021). Mechanical and durability properties of fiber reinforced concrete overlay: Experimental results and numerical simulation. Construction and Building Materials, 268, 121083. https://doi.org/10.1016/j.conbuildmat.2020.121083
- [5] Ravichandran, D., Prem, P. R., Kaliyavaradhan, S. K., & Ambily, P. S. (2022). Influence of fibers on fresh and hardened properties of ultra-high performance concrete (UHPC)—A review. Journal of Building Engineering, 57, 104922. https://doi.org/10.1016/j.jobe.2022.104922
- [6] Soe, K. T., Zhang, Y. X., & Zhang, L. C. (2013). Impact resistance of hybrid-fiber engineered cementitious composite panels. Composite Structures, 104, 320-330. https://doi.org/10.1016/j.compstruct.2013.01.029
- [7] Kafodya, I., & Okonta, F. (2020). Compressive and tensile strength properties of pre-compressed and soaked natural fiber reinforced lime—fly ash stabilised soil. International Journal of Pavement Research and Technology, 13, 497–509. https://doi.org/10.1007/s42947-020-0074-4
- [8] Kanda, T., & Li, V. C. (1998). Interface property and apparent strength of high-strength hydrophilic fiber in cement matrix. Journal of Materials in Civil Engineering, 10(1), 5-13. https://doi.org/10.1061/(ASCE)0899-1561(1998)10:1(5)

- [9] Zarei, A., Rooholamini, H., & Ozbakkaloglu, T. (2022). Evaluating the properties of concrete pavements containing crumb rubber and recycled steel fibers using response surface methodology. International Journal of Pavement Research and Technology, 15, 470–484. https://doi.org/10.1007/s42947-021-00049-7
- [10] Li, V. C., Wu, C., Wang, S., Ogawa, A., & Saito, T. (2002). Interface tailoring for strain-hardening polyvinyl alcohol-engineered cementitious composite (PVA-ECC). Materials Journal, 99(5), 463-472.
- [11] Gillani, S. A. A., Toumi, A., & Turatsinze, A. (2020). Effect of surface preparation of substrate on bond tensile strength of thin bonded cement-based overlays. International Journal of Pavement Research and Technology, 13, 197–204. https://doi.org/10.1007/s42947-019-0101-5
- [12] Li, V. C. (1993). From micromechanics to structural engineering: The design of cementitious composites for civil engineering applications. Doboku Gakkai Ronbunshu, 471, 1-12.
- [13] Li, V. C., Mishra, D. K., & Wu, H. C. (1995). Matrix design for pseudo-strain-hardening fiber reinforced cementitious composites. Materials and Structures, 28, 586-595. https://doi.org/10.1007/BF02473191
- [14] Ahmad, F., Rawat, S., Yang, R. (Chunhui), Zhang, L., Fanna, D. J., Soe, K., & Zhang, Y. X. (2025). Effect of metakaolin and ground granulated blast furnace slag on the performance of hybrid fibre-reinforced magnesium oxychloride cement-based composites. International Journal of Civil Engineering. https://doi.org/10.1007/s40999-025-01074-4
- [15] Asghar, M. F., & Khattak, M. J. (2024). Evaluation of mixture design and tensile characteristics of polyvinyl alcohol (PVA)–fiber reinforced HMA mixtures. International Journal of Pavement Research and Technology, 17, 258–279. https://doi.org/10.1007/s42947-022-00233-3
- [16] Ruan, Y., Han, B., Yu, X., Li, Z., Wang, J., Dong, S., & Ou, J. (2018). Mechanical behaviors of nano-zirconia reinforced reactive powder concrete under compression and flexure. Construction and Building Materials, 162, 663-673. https://doi.org/10.1016/j.conbuildmat.2017.12.063
- [17] Choucha, S., Benyahia, A., Ghrici, M., & Mansour, M. S. (2018). Effect of natural pozzolan content on the properties of engineered cementitious composites as repair material. Frontiers of Structural and Civil Engineering, 12(3), 261-269. https://doi.org/10.1007/s11709-017-0394-x
- [18] Liu, D., Yu, J., Qin, F., Zhang, K., & Zhang, Z. (2023). Mechanical performance of high-strength engineering cementitious composites (ECC) with hybriding PE and steel fibers. Case Studies in Construction Materials, 18, e01961. https://doi.org/10.1016/j.cscm.2023.e01961
- [19] Sobhani, J., & Pourkhorshidi, A. R. (2021). The effects of cold-drawn crimped-end steel fibers on the mechanical and durability of concrete overlay. Civil Engineering Infrastructures Journal, 54(2), 319-330. https://doi.org/10.22059/ceij.2020.297941.1657
- [20] Chompoorat, T., Likitlersuang, S., Buathong, P., Jongpradist, P., & Jamsawang, P. (2023). Flexural performance and microstructural characterization of cement-treated sand reinforced with palm fiber. Journal of Materials Research and Technology, 25, 1570-1584. https://doi.org/10.1016/j.jmrt.2023.06.036
- [21] Buathong, P., Chompoorat, T., Jongpradist, P., Chen, X., & Jamsawang, P. (2023). Effect of palm fiber reinforcement on the unconfined compressive performance of cement-treated sand. Sustainability, 15(11), 8607. https://doi.org/10.3390/su15118607
- [22] Chompoorat, T., Thepumong, T., Nuaklong, P., Jongvivatsakul, P., & Likitlersuang, S. (2021). Alkaliactivated controlled low-strength material utilizing high-calcium fly ash and steel slag for use as pavement materials. Journal of Materials in Civil Engineering, 33(8), 04021178. https://doi.org/10.1061/(ASCE)MT.1943-5533.0003798
- [23] Pakravan, H. R., Jamshidi, M., & Latifi, M. (2016). Study on fiber hybridization effect of engineered cementitious composites with low-and high-modulus polymeric fibers. Construction and Building Materials, 112, 739-746. https://doi.org/10.1016/j.conbuildmat.2016.02.112
- [24] Choi, H. K., Bae, B. I., & Choi, C. S. (2016). Lateral resistance of unreinforced masonry walls strengthened with engineered cementitious composite. International Journal of Civil Engineering, 14, 411-424. https://doi.org/10.1007/s40999-016-0026-1.
- [25] Yao, W., Li, J., & Wu, K. (2003). Mechanical properties of hybrid fiber-reinforced concrete at low fiber volume fraction. Cement and Concrete Research, 33(1), 27-30. https://doi.org/10.1016/S0008-8846(02)00913-4
- [26] Chen, B., & Liu, J. (2005). Contribution of hybrid fibers on the properties of the high-strength lightweight concrete having good workability. Cement and Concrete Research, 35(5), 913-917. https://doi.org/10.1016/j.cemconres.2004.07.035
- [27] Cheng, Y., & Huang, X. (2022). Application of municipal solid waste incineration bottom ash into engineered cementitious composites. International Journal of Pavement Research and Technology, 15, 1106–1117. https://doi.org/10.1007/s42947-021-00075-5

- [28] Kang, S. T., Choi, J. I., Koh, K. T., Lee, K. S., & Lee, B. Y. (2016). Hybrid effects of steel fiber and microfiber on the tensile behavior of ultra-high performance concrete. Composite Structures, 145, 37-42. https://doi.org/10.1016/j.compstruct.2016.02.075
- [29] Meng, W., & Khayat, K. H. (2018). Effect of hybrid fibers on fresh properties, mechanical properties, and autogenous shrinkage of cost-effective UHPC. Journal of Materials in Civil Engineering, 30(4), 04018030. https://doi.org/10.1061/(ASCE)MT.1943-5533.0002212
- [30] Wang, Q., Yi, Y., Ma, G., & Luo, H. (2019). Hybrid effects of steel fibers, basalt fibers and calcium sulfate on mechanical performance of PVA-ECC containing high-volume fly ash. Cement and Concrete Composites, 97, 357-368. https://doi.org/10.1016/j.cemconcomp.2019.01.009
- [31] Zhu, S., Zhang, Y. X., & Lee, C. K. (2024). An experimental study on hybrid fiber reinforced engineered cementitious composite link slabs under static and fatigue loadings. Engineering Structures, 300, 117254. https://doi.org/10.1016/j.engstruct.2023.117254
- [32] Feng, Z., Zhou, Y., Sui, L., & Zhu, Z. (2022). Optimal design of a low-cost high-performance hybrid fiber engineered cementitious composites. Construction and Building Materials, 345, 128372. https://doi.org/10.1016/j.conbuildmat.2022.128372
- [33] Shi, F., Pham, T. M., Hao, H., & Hao, Y. (2020). Post-cracking behavior of basalt and macro polypropylene hybrid fibre reinforced concrete with different compressive strengths. Construction and Building Materials, 262, 120108. https://doi.org/10.1016/j.conbuildmat.2020.120108
- [34] Mehta, P. K. (2002). Greening of the concrete industry for sustainable development. Concrete International, 24(7), 23-28. https://doi.org/10.1016/j.cemconcomp.2008.12.010
- [35] Malhotra, V. M. (2000). Role of supplementary cementing materials in reducing greenhouse gas emissions. Concrete Technology for a Sustainable Development in the 21st Century, 5, 6.
- [36] Torres, A., Brandt, J., Lear, K., & Liu, J. (2017). A looming tragedy of the sand commons. Science, 357(6355), 970-971. https://doi.org/10.1126/science.aao0503
- [37] Zhang, L., Liu, W., Wang, L., & Ling, Z. (2020). On-axis and off-axis compressive behavior of pultruded GFRP composites at elevated temperatures. Composite Structures, 236, 111891. https://doi.org/10.1016/j.compstruct.2020.111891
- [38] Kim, J. K., Kim, J. S., Ha, G. J., & Kim, Y. Y. (2007). Tensile and fiber dispersion performance of ECC (engineered cementitious composites) produced with ground granulated blast furnace slag. Cement and Concrete Research, 37(7), 1096-1105. https://doi.org/10.1016/j.cemconres.2007.04.006
- [39] Sumukh, E. P., Das, B. B., & Barbhuiya, S. (2024). Synergy of hydration and microstructural properties of sustainable cement mortar supplemented with industrial by-products. International Journal of Civil Engineering, 22(7), 1137-1158. https://doi.org/10.1007/s40999-024-00950-9
- [40] Qiu, J., Tan, H. S., & Yang, E. H. (2016). Coupled effects of crack width, slag content, and conditioning alkalinity on autogenous healing of engineered cementitious composites. Cement and Concrete Composites, 73, 203-212. https://doi.org/10.1016/j.cemconcomp.2016.07.013
- [41] Zhu, Y., Zhang, Z., Yang, Y., & Yao, Y. (2014). Measurement and correlation of ductility and compressive strength for engineered cementitious composites (ECC) produced by binary and ternary systems of binder materials: Fly ash, slag, silica fume and cement. Construction and Building Materials, 68, 192-198. https://doi.org/10.1016/j.conbuildmat.2014.06.080
- [42] Zhang, J., Wang, Q., & Wang, Z. (2016). Optimizing design of high strength cement matrix with supplementary cementitious materials. Construction and Building Materials, 120, 123-136. https://doi.org/10.1016/j.conbuildmat.2016.05.100
- [43] Liu, Y., Zhou, X., Lv, C., Yang, Y., & Liu, T. (2018). Use of silica fume and GGBS to improve frost resistance of ECC with high-volume fly ash. Advances in Civil Engineering, 2018(1), 7987589. https://doi.org/10.1155/2018/7987589
- [44] Wang, Q., Lai, M. H., Zhang, J., Wang, Z., & Ho, J. C. M. (2020). Greener engineered cementitious composite (ECC)—The use of pozzolanic fillers and unoiled PVA fibers. Construction and Building Materials, 247, 118211. https://doi.org/10.1016/j.conbuildmat.2020.118211
- [45] ASTM C31-22. (2022). Standard Practice for Making and Curing Concrete Test Specimens in the Field. ASTM International, West Conshohocken, PA.
- [46] ASTM C511-22. (2022). Standard Specification for Mixing Rooms, Moist Cabinets, Moist Rooms, and Water Storage Tanks Used in the Testing of Hydraulic Cements and Concretes. ASTM International, West Conshohocken, PA.
- [47] ASTM C231-22. (2022). Standard Test Method for Air Content of Freshly Mixed Concrete by the Pressure Method. ASTM International, West Conshohocken, PA.
- [48] ASTM C138-22. (2022). Standard Test Method for Density (Unit Weight), Yield, and Air Content (Gravimetric) of Concrete. ASTM International, West Conshohocken, PA.

International Journal of Multiphysics

Volume 18, No. 4, 2024

ISSN: 1750-9548

- [49] BS EN 12390-3. (2019). Standard Test Method for Compressive Strength of Cement Mortar. ASTM C1116 / C1116M-10a. (2015). Standard Specification for Fiber-Reinforced Concrete. ASTM International, West Conshohocken, PA.
- [50] ASTM C1609/C1609M-19a. (2019). Standard Test Method for Flexural Performance of Fiber-Reinforced Concrete (Using Beam with Third-Point Loading). ASTM International, West Conshohocken, PA.
- [51] ASTM C496/C496M. (2017). Standard test method for splitting tensile strength of cylindrical concrete specimens. ASTM International, West Conshohocken, PA.
- [52] ASTM C469. (2002). Standard Test Method for Static Modulus of Elasticity and Poisson's Ratio of Concrete in Compression. ASTM International.
- [53] EN 12390-8. (2009). Testing hardened concrete Part 8: Depth of penetration of water under pressure. European Committee for Standardization.
- [54] DIN EN 1338. (2003). Concrete paving blocks Requirements and test methods. Deutsches Institut für Normung.
- [55] ASTM C1202. (2012). Standard Test Method for Electrical Indication of Concrete's Ability to Resist Chloride Ion Penetration. ASTM International.
- [56] AASHTO T358. (2015). Standard Method of Test for Surface Resistivity Indication of Concrete's Ability to Resist Chloride Ion Penetration. American Association of State Highway and Transportation Officials.
- [57] Iranian Concrete Code Volume II Materials and Construction, No.120-2. (2021). Last Edition, 22/11/2021.
- [58] Bremner, T. W., Hover, K. C., Poston, R. W., Broomfield, J. P., Joseph, T., Price, R., et al., editors. (2001). Protection of metals in concrete against corrosion ACI 222 R-01. Reported by ACI Committee 222.
- [59] Zhu, H., Zhang, D., Wang, T., McBain, M., & Li, V. C. (2021). Intrinsic self-stressing and low carbon Engineered Cementitious Composites (ECC) for improved sustainability. Cement and Concrete Research, 149, 106580. https://doi.org/10.1016/j.cemconres.2021.106580
- [60] Lee, K. M., & Park, P. J. (2005). Estimation of the environmental credit for the recycling of granulated blast furnace slag based on LCA. Resources, Conservation and Recycling, 44(2), 139-151. https://doi.org/10.1016/j.resconrec.2004.11.004
- [61] Waqar, A., Khan, M. B., Afzal, M. T., Radu, D., Gălățanu, T., Cazacu, C. E., & Almujibah, H. R. (2024). Investigating the synergistic effects of carbon fiber and silica fume on concrete strength and eco-efficiency. Case Studies in Construction Materials, 20, e2967. https://doi.org/10.1016/j.cscm.2024.e02967